INVESTIGATION ON AIRCRAFT AERODYNAMICS IN GUSTY INFLOW CONDITIONS

By

Malungelo Luzipho

*A thesis submitted to the College of Aerospace Engineering in conformity with the requirements for the degree of **Bachelor of Engineering**.*

Nanjing University of Aeronautics & Astronautics
Nanjing, Jiangsu Province, People's Republic of China

June 2021

Supervised by

Prof. Zhenlong Wu

ABSTRACT

The use of computational fluid dynamics (CFD) software in engineering industries has increased gradually over the years. The need for more advanced technology and sustainability measures in the field of aerospace has exacerbated the growth in the learning of the various CFD package software modules. An aircraft encounters gust or turbulence, as it is commonly known, at various stages of flight. The study of how aircraft surfaces such as the wing interact and react to this turbulence is an area in which research has increased over the years.

Two types of inflow conditions exist, namely: Sears inflow conditions and Atassi inflow conditions. They are associated with two respective transfer functions, Sears and Atassi transfer functions. In aircraft aerodynamics, lift is generated by the way air flows around the wing, which is known scientifically as an airfoil. The purpose of the two previously mentioned transfer functions is to provide illustrative visualisations for the unsteady lift responses of a test airfoil. Oscillating grid vanes were used to generate an Atassi gust and a Sears gust for the respective cases of computational fluid dynamics (CFD). This thesis gives a comprehensive study on how factors such as frequency, gust angle and freestream velocity affect the lift response of the test airfoils. Furthermore, analysis is provided on how the aerodynamic coefficients are affected when the test airfoils are subjected to the aforementioned inflow conditions. Results obtained in this thesis were mainly compared with those obtained in the work previously done by different groups of researchers, in a similar fashion.

Three test cases were run using OpenFOAM software and were compared using Reynolds-Averaged Simulations (RAS). The advantage of using the aforementioned software is its ease of use and understanding.

KEYWORDS: Computational Fluid Dynamics (CFD), Transfer Function, Aerodynamics, Gust, Sears, Atassi, Turbulence

Contents

LIST OF FIGURES

Figure 4.1(a): Velocity magnitude profile for the Atassi gusty inflow at t/T = 1/8, together with the flow field of the freestream velocity (U_∞ = 25m/s), frequency f = 5Hz and gust angle α_g = 2°.

Figure 4.1(b): At t/T = 1/4. Image shows position of the oscillating vanes halfway through the first oscillation. The vanes take a more linear shape across the horizontal axis hence showing movement from the initial angle position in Fig. 12(a).

Figure 4.1(c): The focused protocol for the Atassi inflow at t/T = 3/8, together with the flow field of the freestream velocity (U_∞ = 25m/s), frequency f = 5Hz and gust angle α_g = 2°.

Figure 4.1(d): The positional structure of the oscillating vanes at t/T = 1/2. The velocity flow field is shown for the same parameters as those shown in Fig. 12(a).

Figure 4.1(e): The positional structure of the oscillating vanes at t/T=5/8. The velocity flow field is shown for the same parameters as those shown in Fig. 12(a).

Figure 4.1(f): The positional structure of the oscillating vanes at t/T=3/4. The velocity flow field is shown for the same parameters as those shown in Fig. 12(a).

Figure 4.1(g): The positional structure of the oscillating vanes at t/T=7/8. The velocity flow field is shown for the same parameters as those shown in Fig. 12(a). Fourth vane from the top shows a high pressure point at the leading edge which yields an increase in the velocity.

Figure 4.1(h): The positional structure of the oscillating vanes at t/T=1. The velocity flow field is shown for the same parameters as those shown in Fig. 12(a). Deflection of oscillating vanes results in an increase in the magnitude of the velocity at the leading edge of the top/first vane.

Figure 4.2(a): Average trajectory of the streamlines of the velocity flow field when the 4 oscillating vanes rotate through an angle of 2° upward from the position in Fig. 13(b) for focused protocol (Case 1) with frequency, f = 5Hz.

Figure 4.2(b): Average trajectory of the streamlines of the velocity flow field when the 4 vanes maintain a similar flat, horizontal position after deflection, for focused protocol (Case 1) with frequency, f = 5Hz.

Figure 4.2(c): Average trajectory of the streamlines of the velocity flow field when the 4 oscillating vanes rotate through an angle of 2° downward from the position in Fig. 13(b) for focused protocol (Case 1) with frequency, f = 5Hz.

Figure 4.3(a): Velocity magnitude profile for the Atassi gusty inflow at the start of one oscillation period, t/T=0, together with the flow field of the freestream velocity (U_∞ = 25m/s), frequency f = 8Hz and gust angle α_g = 2°.

Figure 4.3(b): Velocity magnitude profile for the Atassi gusty inflow at the start of one oscillation period, t/T=1/5, together with the flow field of the freestream velocity (U_∞ = 25m/s), frequency f = 8Hz and gust angle α_g = 2°.

Figure 4.3(c): Velocity magnitude profile for the Atassi gusty inflow at the start of one oscillation period, t/T=2/5, together with the flow field of the freestream velocity (U_∞ = 25m/s), frequency f = 8Hz and gust angle α_g = 2°. Velocity flow field is shown along with the position of the oscillating vanes.

Figure 4.3(d): Velocity magnitude profile for the Atassi gusty inflow at the start of one oscillation period, t/T=3/5, together with the flow field of the freestream velocity (U_∞ = 25m/s), frequency f = 8Hz and gust angle α_g = 2°.

Figure 4.3(e): Velocity magnitude profile for the Atassi gusty inflow at the start of one oscillation period, t/T=4/5, together with the flow field of the freestream velocity (U_∞ = 25m/s), frequency f = 8Hz and gust angle α_g = 2°.

Figure 4.3(f): Velocity magnitude profile for the Atassi gusty inflow at the start of one oscillation period, t/T=1, together with the flow field of the freestream velocity (U_∞ = 25m/s), frequency f = 8Hz and gust angle α_g = 2°.

Figure 4.4(a): Average trajectory of the streamlines of the flow field with respect to freestream velocity, U_∞, at a first instance for focused protocol (Case 2) with frequency, f = 8Hz.

Figure 4.4(b): Average trajectory of the streamlines of the flow field with respect to freestream velocity, U_∞ at a second instance for focused protocol (Case 2) with frequency, f = 8Hz.

Figure 4.4(c): Average trajectory of the streamlines of the flow field with respect to freestream velocity, U_∞, at a third instance for focused protocol (Case 2) with frequency, f = 8Hz.

Figure 4.5(a): Velocity magnitude profile for the Sears gusty inflow at t/T = 0, together with the flow field of the freestream velocity (U_∞ = 20m/s), frequency f = 8Hz and gust angle α_g = 2°.

Figure 4.5(b): Velocity magnitude profile for the Sears gusty inflow at t/T = 1/2, together with the flow field of the freestream velocity (U_∞ = 20m/s), frequency f = 8Hz and gust angle α_g = 2°.

Figure 4.6: Average path of the streamlines of the flow field with respect to freestream velocity, U_∞, for limited protocol (Case 3) with frequency, f = 8Hz.

Figure 4.7(a): Plotted graph shows how the pitching moment coefficient (C_m) varied with time over the course of the simulation.

Figure 4.7(b): Plotted graph shows how the drag coefficient (C_d) varied with time over the course of the simulation.

Figure 4.7(c): Plotted graph shows how the lift coefficient (C_L) varied with time over the course of the simulation.

Figure 4.8(a): Plotted graph shows how the pitching moment coefficient (C_m) varied with time over the course of the Atassi gust for a frequency of f = 8Hz & freestream velocity of U_∞ = 25m/s.

Figure 4.8(b): Plotted graph shows how the drag coefficient (C_d) varied with time over the course of the simulation for a frequency of f = 8Hz & freestream velocity of U_∞ = 25m/s.

Figure 4.8(c): Plotted graph shows how the lift coefficient (C_L) varied with time over the course of the simulation for a frequency of f = 8Hz & freestream velocity of U_∞ = 25m/s.

Figure 4.9(a): Plotted graph shows how the pitching moment coefficient (C_m) varied with time over the course of the sears gust for a frequency of f = 8Hz & freestream velocity of U_∞ = 20m/s.

Figure 4.9(b): Plotted graph shows how the drag coefficient (C_d) varied with time over the course of the simulation for a frequency of f = 8Hz & freestream velocity of U_∞ = 20m/s.

Figure 4.9(c): Plotted graph shows how the lift coefficient (C_L) varied with time over the course of the simulation for a frequency of f = 8Hz & freestream velocity of U_∞ = 20m/s.

LIST OF TABLES

NOMENCLATURE

Symbol	***Definition [Units]***
°	*Degree/s. [Unit of Measurement]*
U	*Gust Velocity [m/s]*
V	*Aircraft Forward Flight Speed [m/s]*
V_e	*Aircraft Effective Velocity [m/s]*
v	*Normal Velocity Component.*
u	*Streamwise Velocity Component.*
f	*Frequency/Vane Oscillation Frequency. [Hz]*
k_1	*First Reduced Frequency. [Hz]*
k_2	*Second Reduced Frequency. [Hz]*
f_1	*First Dimensional Frequency. [Hz]*
f_2	*Second Dimensional Frequency. [Hz]*
c	*Airfoil Chord length. [m]*
α_0	*Installation Angle. [°]*
α_g	*Gust Angle/Angle of Attack Variations. [°]*
$\tilde{\alpha}_g$	*Gust Angle Amplitude/Specific Gust Angle. [°]*
U_∞	*Freestream Velocity. [m/s]*
h_L	*Transfer Function.*
L_{us}	*Unsteady Lift.*
L_{qs}	*Quasi-Steady Lift.*
$\tilde{L}_{us}$	*Unsteady Lift Amplitude.*
$\tilde{L}_{qs}$	*Quasi-Steady Lift Amplitude.*
$e^{\emptyset i}$	*Phase Shift Between Dynamic and Quasi-Steady Lift Force Signals.*
e	*Exponent.*
$\tilde{v}$	*Vertical Velocity Fluctuation Amplitude.*
$\tilde{u}$	*Streamwise Velocity Fluctuation Amplitude.*
π	*Mathematical Constant (Pi).*
α	*Airfoil Camber.*
η	*Angle of Attack. [°]*

P_1	*Velocity Probing Position at the Leading Edge of Test Airfoils.*
P_2	*Velocity Probing Position at the Fixed Point.*
s	*Space Between Adjacent Vanes. [m]*
b	*Vertical Length of Grid. [m]*
$\tilde{\theta}$	*Vane Oscillation Amplitude. [°]*
C	*Constant at the Same Grid Oscillation Frequency.*
$\tilde{\theta}_{req}$	*Required Vane Oscillation Amplitude. [°]*
$\emptyset_g$	*Gust Phase Shift. [°]*
$G_{vv}(f)$	*Spectral Density of Turbulent Velocity Upstream of Airfoil.*
$A_{vv}(f)$	*Spanwise Correlation Length of the Turbulent Velocity. [m]*
$H(f)$	*Gust Response Function.*
f_e	*Characteristic Frequency of the Energy Containing Eddies. [Hz].*
L_{11}	*Longitudinal Integral Length Scale of the Turbulence. [m]*
V_{rms}	*Root Mean Square Velocity. [m/s]*
$S(k)$	*Sears Function.*
ρ	*Variation of Lift Coefficient with Angle of Wind Incidence.*
τ	*Maximum Thickness.*
β	*Thickness Factor.*
B	*Variation of Lift Coefficient with Angle of Wind Incidence.*
$\bar{V}$	*Variation of Lift Coefficient with Angle of Wind Incidence.*
C_Z	*Variation of Lift Coefficient with Angle of Wind Incidence.*
C_Z'	*Variation of Lift Coefficient with Angle of Wind Incidence.*
f_j^*	*Reduced Frequency. [Hz]*
$S_{F_z,u,w}$	*Terms for the Power Spectral Density of the Wind Components.*
$\lvert\Phi_Z(f^*)\rvert^2$	*Aerodynamic (Lift) Admittance of a Thin Airfoil.*
Δ_y	*Span-Wise Distance. [m]*
$S_{L_1L_2}/S_L$	*Normalized Cross-Spectrum of Lift Force Between 2 strips.*
μ_j	*The jth Mode Shape.*
Γ	*Euler Gamma Function.*
Cm	*Pitching Moment Coefficient.*
Cd	*Drag Coefficient.*
C_L	*Lift Coefficient.*

L/D	*Lift-to-Drag Ratio.*
t	*Time. [s]*
T	*Period. [s]*
δ	*Aspect Ratio.*
A_{2D}	*Two-Dimensional Aerodynamic Admittance.*
A_{3D}	*Three-Dimensional Aerodynamic Admittance.*
$\mathbf{u}$	*3D Velocity Field.*
$\mathbf{g}$	*Vector of the Acceleration Due to Gravity.* $[m/s^2]$
σ	*Shear Stress Tensor.* $[N/m^2]$
e	*Total Specific Energy. [J/kg]*
Q	*Volume Energy Source.*
q	*Heat Flux.*
$\boldsymbol{\rho}$	*Density of Fluid.* $[kg/m^3]$
Γ	*Diffusivity.* $[m^2/s]$
ϕ	*Generic Scalar.*
∇	*Gradient/Divergence Factor.*

Abbreviations

CFD	*Computational Fluid Dynamics.*
FOAM	*Field Operation And Manipulation.*
AOA	*Angle of Attack.*
URANS	*Unsteady Reynolds Averaged Navier-Stokes.*
SST	*Shear Stress Transport.*
PIV	*Particle Image Velocimetry.*
NACA	*National Advisory Committee of Aeronautics.*
RAS	*Reynolds Averaged Simulation.*
ABL	*Atmospheric Boundary Layer.*
POD	*Proper Orthogonal Decomposition.*
FVM	*Finite Volume Method.*

Chapter 1: INTRODUCTION

1.1 Background & Meaning

Literature Review

When an aircraft is in full motion (in flight) it encounters a lot of forces, mainly against the airframe of the vehicle. These forces are a result of air particles hitting the surfaces of the plane as it moves and therefore affecting its movement too. Some are minimal and some may be extreme. The latter is true in the case of turbulence being experienced by the aircraft. Turbulence is caused by different factors. These include flying through severe thunderstorms (upward and downward currents) and thermal currents. The most hazardous type of turbulence is clear air turbulence which is brought up by rapidly changing wind speed or direction. What makes it dangerous is the fact that it occurs in clear skies with perfect visibility and therefore cannot be picked by the weather radar. These come under the scientific classification of ‘gust’. A brief summary on how pilots can counter these external forces (gusty winds) is given further below. As the years have gone by, adequate literature and reviews have been provided pertaining to the research that has been conducted and published thereby showing an increase in efforts to try to understand this subject [1].

Having mentioned this, the research carried out for this thesis was centred around the main topic of: “Investigation of Aircraft aerodynamics in Gusty Inflow Conditions”. To give a clear and concise understanding of the topic, the following definitions are given,

- **Gust** – Strong wind blowing against a moving object in through the air.
- **Aerodynamics** – The study of how air moves around stationary and moving objects. It includes the understanding of how aircraft are able to fly.

The use of Computational Fluid Dynamics (CFD) software such as OpenFOAM is necessary to run simulations in an attempt to grasp certain concepts of aerodynamics and to see how various fluids move around vehicle bodies e.g aircraft, ship propellers & rotor blades, automobiles etc. This includes compressible and incompressible flow of fluids.

Flight control surfaces (*Rudder, ailerons, flaps, horizontal and vertical stabilizers*) need to be fully functional to enable an aircraft to manoeuvre under normal flight conditions & operations (*take-off, cruise, loiter & landing/touchdown*), and to ensure that, under turbulent circumstances or conditions, the pilot can maintain the plane’s stability and avoid it stalling.

To briefly illustrate the different variations of gust with respect to direction, an image is shown below.

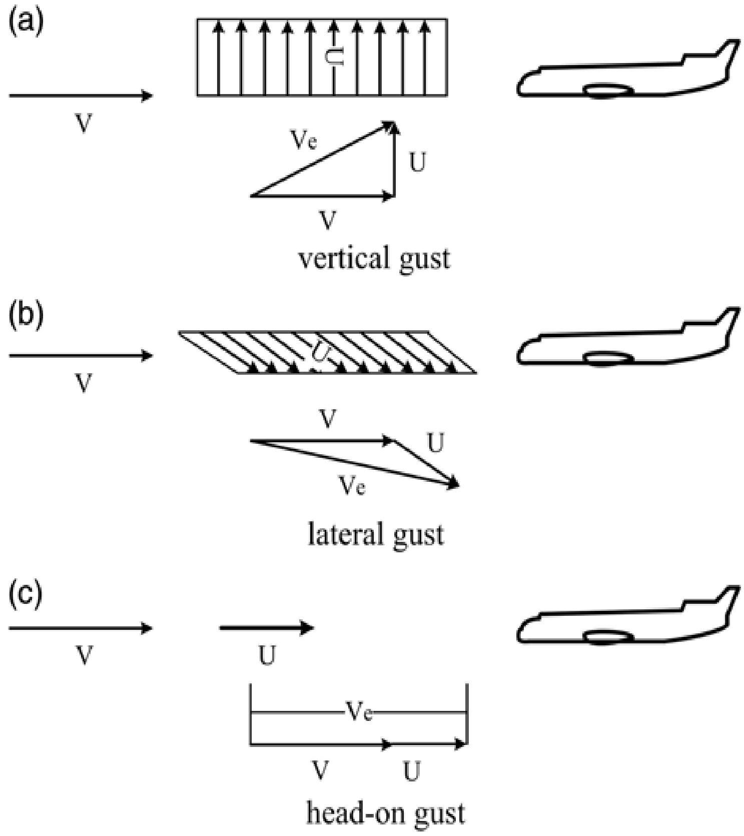

Figure 1.1: Illustration of gust directionality. (Figure from Reference [1])

Directionality – As seen in Fig. 1 above, there are three types of gust. Namely, vertical, lateral and head-on gust. Vertical gust is equal to the change of attack while lateral gust is equal to the change in side-slip angle and head-on gust is equal to the dynamic pressure of the aircraft. The singular directional components of gust velocity at orthogonal angles to the flight path are the main cause of this. In the image above, $\boldsymbol{U}$ is the gust velocity, $\boldsymbol{V}$ is the aircraft forward flight speed and $\boldsymbol{V_e}$ is the aircraft effective velocity [1].

1.1.1 *Sears, Atassi* & Theodorsen Functions

The figures below illustrate the periodic velocity changes/fluctuations in the component normal to the airfoil (v) and in the streamwise velocity component (u) respectively.

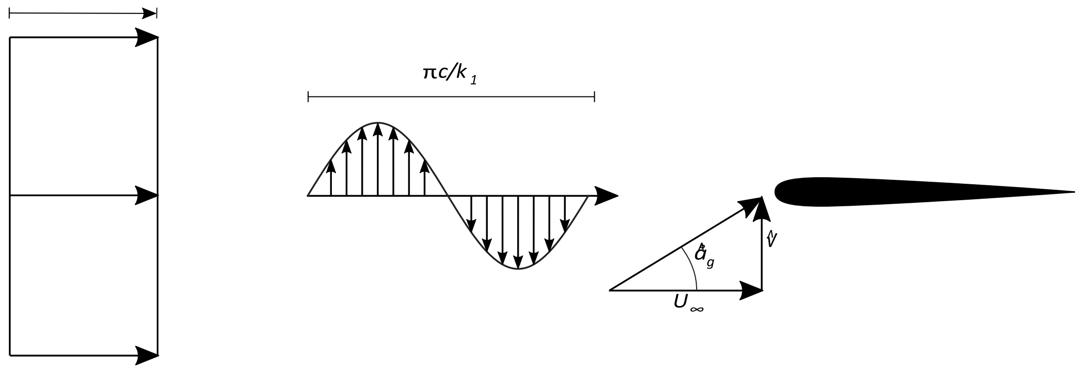

Figure 1.2: Figure shows the Sears inflow conditions and the fluctuations in the normal velocity component v with reduced frequency k_1 affect the airfoil. Alpha g symbolizes the variations of the angle of attack (AOA). (Figure from Reference [2])

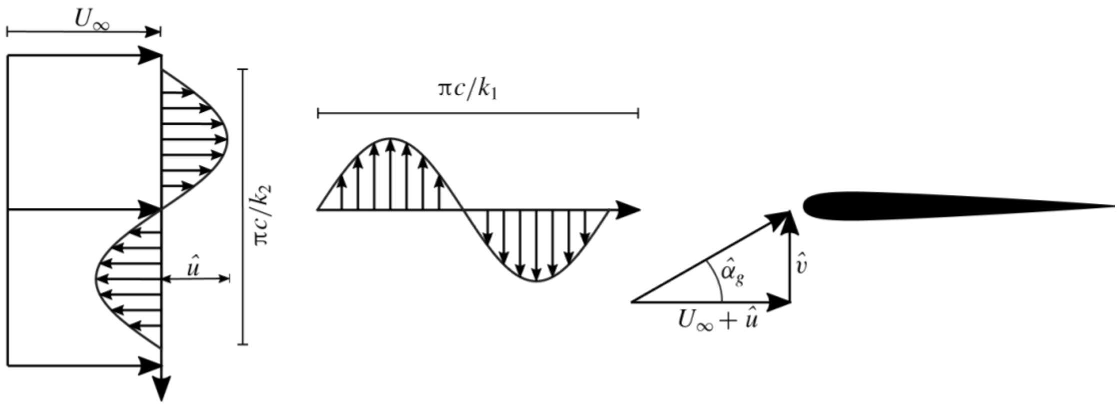

Figure 1.3: Figure shows the Atassi inflow condition. The following parameters are seen in the model above: Streamwise velocity fluctuations that have an amplitude equal to u & a minimized frequency equal to k_2. The Sears problem gust is adjoined to the added gust profile as seen above. (Figure from Reference [2])

Sears, Atassi and Theodorsen functions are investigated in this paper but the main focus will be on the former (Sears & Atassi). This is to give a clear understanding of their operations and applications. The Theodorsen and Sears functions are dependent on the reduced frequency of incoming gust. The Sears function is extracted from the Kutta-Joukowski Theorem and is vastly used in the prediction of unsteady loads in gust-response problems. It was later extended by Goldstein and Atassi and this process led to the formulation of the Atassi function [2]. The expansion process was carried out using 2^{nd}-order models to account for the distortion of the flow field and gust due to the presence of an airfoil. Therefore, it can be deduced that the Atassi function is a 2^{nd}-order model [2].

Based on research conducted in past times, it has been seen that the Atassi function is capable of accounting for the effects of flow changes in normal and streamwise directions. Moreover, the effect of airfoil thickness was not considered because of the stagnation point at the leading edge which made it more difficult. The Sears function was modified further by Lysak *et al* (2013) for predicting the unsteady lift forces. The effect of thickness was taken into account for larger frequencies. The topic of Aerodynamic Admittance, an important aspect to study in relation to the aforementioned functions, is briefly reviewed and described ahead. Reference [4] carried out an experiment to analyse the fluctuating lift of a rigid wing in turbulent flow. In addition to this, the turbulent fluctuations and the power spectra of the lift were measured. A conventional analytical approach factoring in the three-dimensional effects of turbulence on the two wavenumber spectrum and the aerodynamic admittance of the lift-force on an airfoil was put forward by Li *et al* (2015).

Regarding the Sears function, an uncomplicated function can be deduced by changing the gust reference to the leading edge from the initial mid-chord position of the airfoil. It was seen by Giesing *et al* (1970) that this function allows for the precise addition of the large number of reduced frequencies needed in the study of gust frequency response. A phenomenon that has been observed by many researchers is that of wind turbines being subjected to what is called an Atmospheric Boundary Layer (ABL). It is characterized by turbulent winds that create a myriad of aerodynamic circumstances at the rotor in a matter of seconds [7]. Traphan *et al* (2018) analysed an airfoil that was subjected to a vertical and longitudinal gust. The paramount use of a stochastic method called ‘Proper Orthogonal Decomposition’ (POD) for this investigation enabled the researchers to observe the existence of a three-dimensional flow variation along the span of the test airfoil [7]. The work done by Traphan *et al* (2018) sheds light on a different approach that can be implemented in the investigation of the aerodynamic behaviour of an airfoil under turbulent/gusty inflow conditions (tailored).

Reference [8] carried out an investigation and experimental research similar to the one shown in this paper. Wu *et al* (2020) performed an experiment to provide insights into the response of an airfoil to sinusoidal gusty inflow created by oscillating vanes. There was use of a closed loop wind tunnel which made the overall assessment feasible. Harmonic inflow angle variations were exerted at the location of the test airfoil so as to attain varied results for study [8]. There exists a similarity between the above-noted analysis and the one in this paper, which is that, two different protocols were applied to monitor the time varying motion of the respective vanes belonging to the active grid which was numerically computed. They are focused protocol and limited protocol. Their purpose was to solve the Atassi inflow conundrum and, to achieve the gust condition for the Sears inflow problem, respectively [8]. Parameters such as the gust angle (denoted by α_g) in gust response analysis for the two respective inflows, have a somewhat large bearing on the outcome and results of the simulations and experiment. A reduced frequency results in a reduced gust angle. Test airfoils respond slightly differently to each type of inflow condition with small discrepancies in parameter values. More details about the Atassi problem are found in an identical experiment performed by Wei *et al* (2019).

An important point to note is that, in the above-mentioned work done by Wei *et al* (2019), a PIV experiment was carried out in an attempt to gather results from the various occurrences within the flow field. The similarity of the work done by Wu *et al* (2020) and Wei *et al* (2019) gives room for comparison of results achieved by the former, which was done, for the sole purpose of clarification.

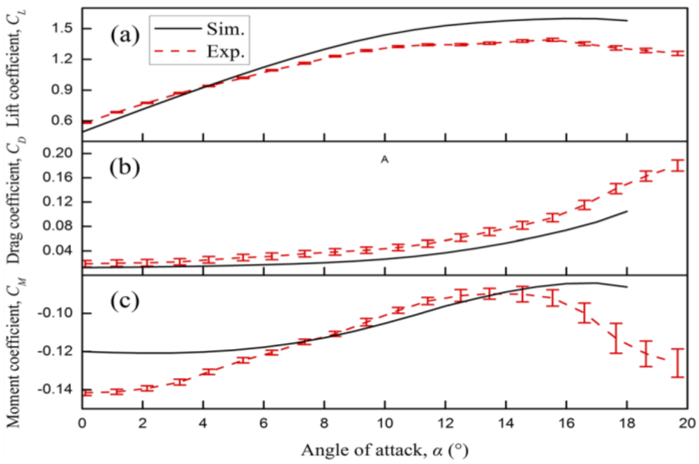

Figure 1.4: The Simulation and Experimental results are represented by the black and red curves, respectively. Results are for (a) lift, (b) drag & (c) pitching moments coefficients. The dashed red curve also shows the mean value and the error bars show the standard deviation around the measured mean value. (Figure from Reference [8])

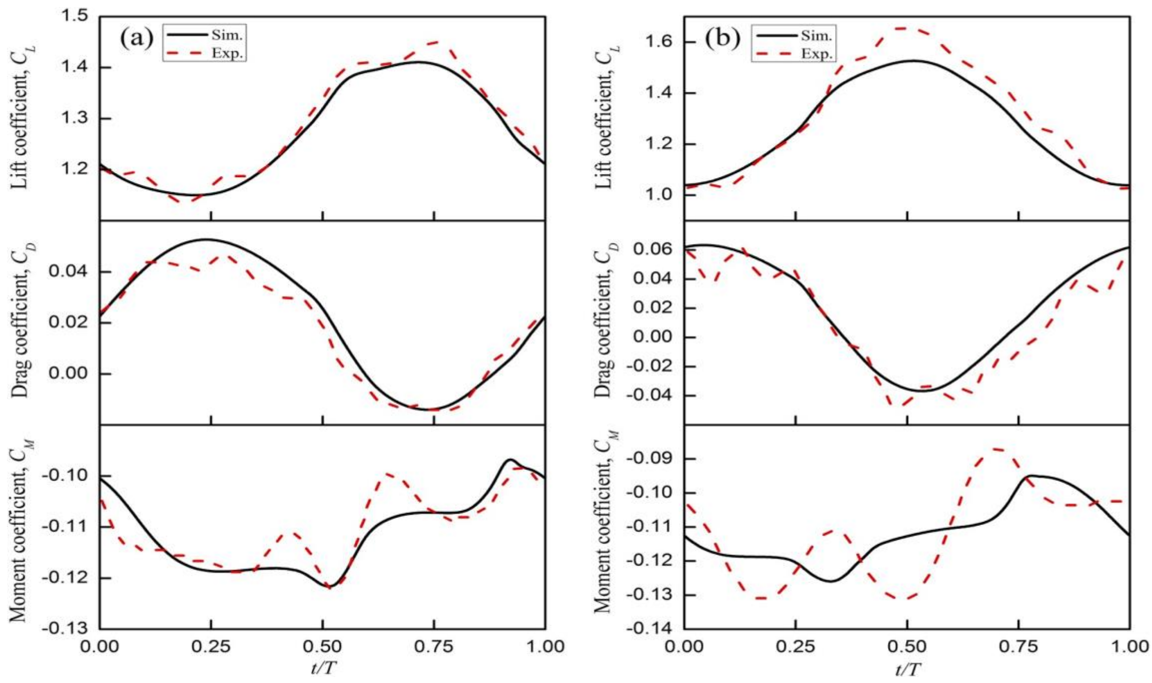

Figure 1.5: Measurement of the lift, drag & pitching moment coefficients and their variation with time (t) at certain periods (T) for the grid vane frequency of (a) f = 5Hz & (b) f = 8Hz. Additional parameters are the constant grid vane amplitude of $\tilde{\theta}$ = 8° & a freestream velocity value of U_∞ = 25m/s. (Figure from Reference [8])

The following images in Fig. 6 give a clear, schematic illustration of the numerical and computational set-up of the experiment conducted by Wu *et al* (2020). Two active grids are seen. In (a), the grid contains six oscillating vanes which are seen to be applied and this happens with a simple sinusoidal oscillation ($\tilde{\theta}$) along the quarter chord-point. In (b), the grid contains four oscillating vanes which are seen to be fixed with a non-zero average angle. The reason for this is to ensure that the flow is limited to the desired section of the airfoil being tested. This setup is identical to the one examined and executed in this paper. Chapter 4 clarifies and supplements this concept.

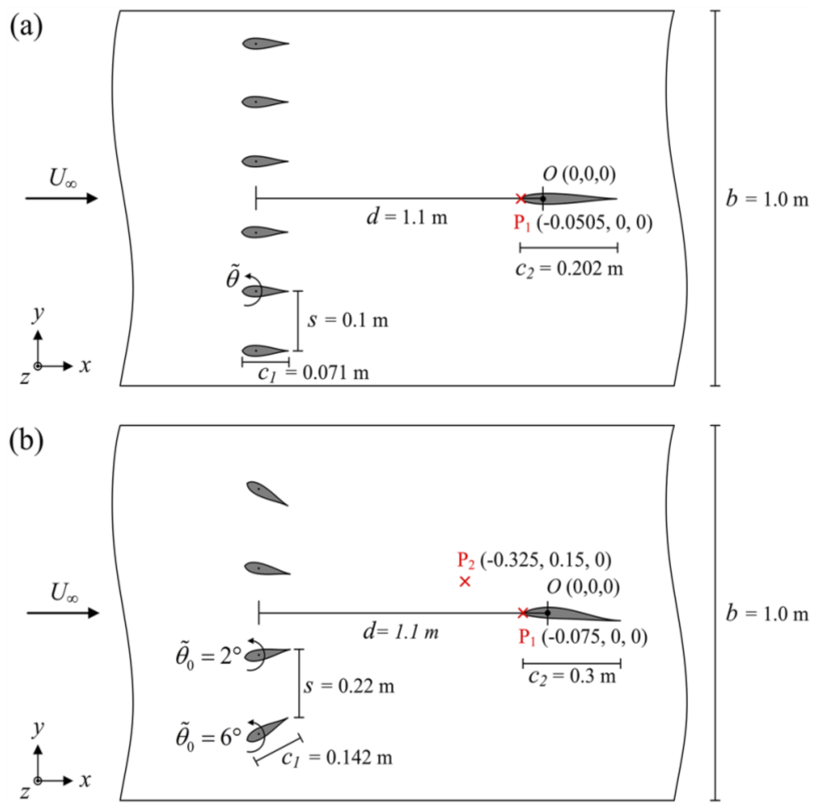

Figure 1.6: (a) Sears inflow condition produced by Limited Protocol (b) Atassi inflow condition produced by Focused Protocol. (Figure from Reference [8])

1.1.2 Additional Information on Theodorsen & Sears Functions

According to Cordes *et al* (2017), the Theodorsen function is a good estimator for the unsteady lift at moderate mean angles of attack. Another experiment was conducted by Cordes *et al* (2017) to observe how these two transfer functions (Theodorsen & Sears) work for an oscillating airfoil and sinusoidal vertical gust. Consequently, It was seen that some results were not consistent with the theories i.e Sears theory, while the experimental results for the Theordorsen function were consistent with the theories pertaining to it. Reference can be made to [9] for further detailed information regarding this process.

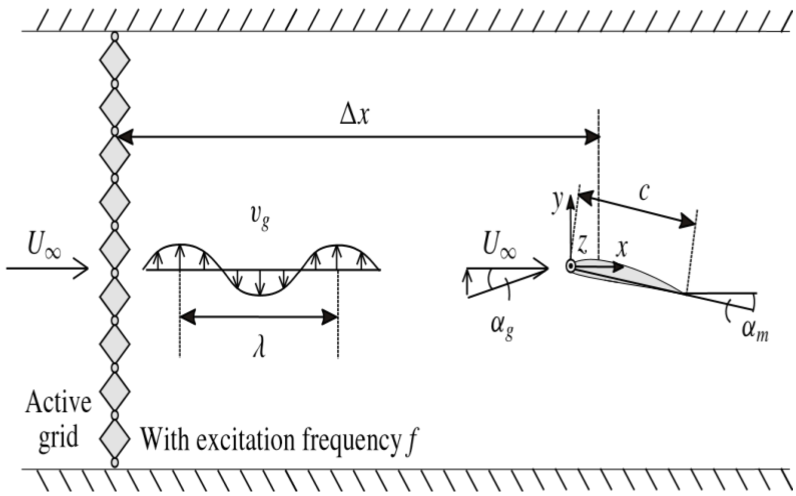

Figure 1.7: Experimental setup showing the top view of the rigid airfoil subjected to a vertical sinusoidal gust. (Figure from Reference [9])

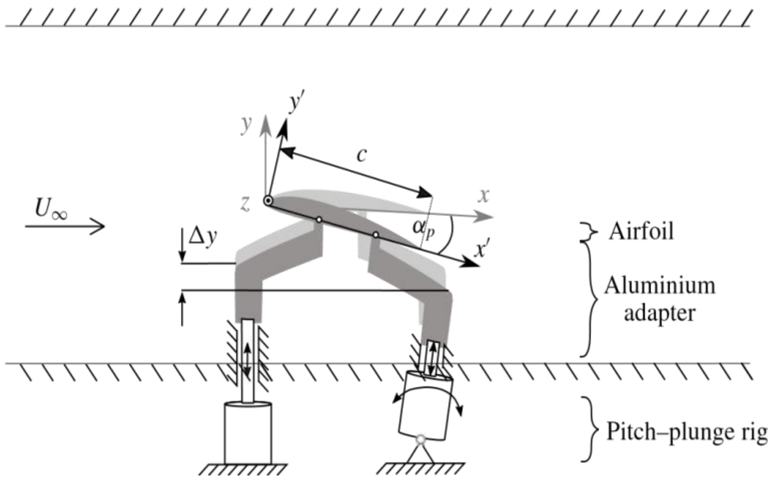

Figure 1.8: Experimental setup showing the side view of the pitching airfoil subjected to a steady air stream. (Figure from Reference [9])

1.2 Aerodynamic Admittance

An important phenomenon and aspect of study to better understand the subject of aerodynamics with a particular focus on the transfer functions is that of aerodynamic admittance. By definition, the aerodynamic admittance is a frequency based transfer function which relates the velocity fluctuations in a turbulent wind to the transverse (cross-wind) force fluctuations experienced by a certain structure subjected to that wind. The structure can range from an aircraft/aircraft wings in motion to tall buildings, large wind turbine blades and long span bridges. Research has been done in the past to show how aspect ratio and the turbulence length scale effect the 'Strip theory approximation'. The aerodynamic admittance can be partitioned into two-dimensional aerodynamic admittance A_{2D} and three-dimensional aerodynamic admittance A_{3D}. Massaro and Graham (2015) analysed the three-dimensional effects of turbulence on a thin airfoil strip. The conclusive evidence proved that, for large aspect ratios, the influence of spanwise wavenumber is negligible for the aerodynamic admittance of buffeting forces. Fig. 6 & 7 show the results obtained from the computation of the respective functions analysed by Massaro and Graham (2015). A modification that enabled the Sears function to account for the three-dimensional effects of finite span sections was brought up by reference [10]. For further results on the investigation conducted by the aforementioned researchers, reference can be made to [10].

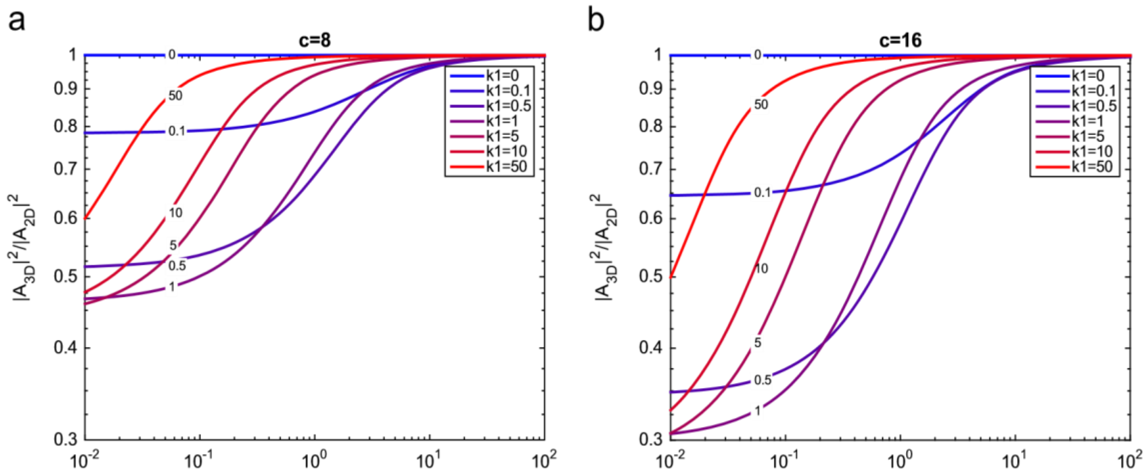

Figure 1.9: Ratio of the 2D & 3D aerodynamic admittance as a function of the aspect ratio δ, for a different reduced frequency k_1 and the different correlation c. Retrieved from Reference [10].

- 2D & 3D aerodynamic admittance → *y-axis*
- Aspect ratio δ → *x-axis*

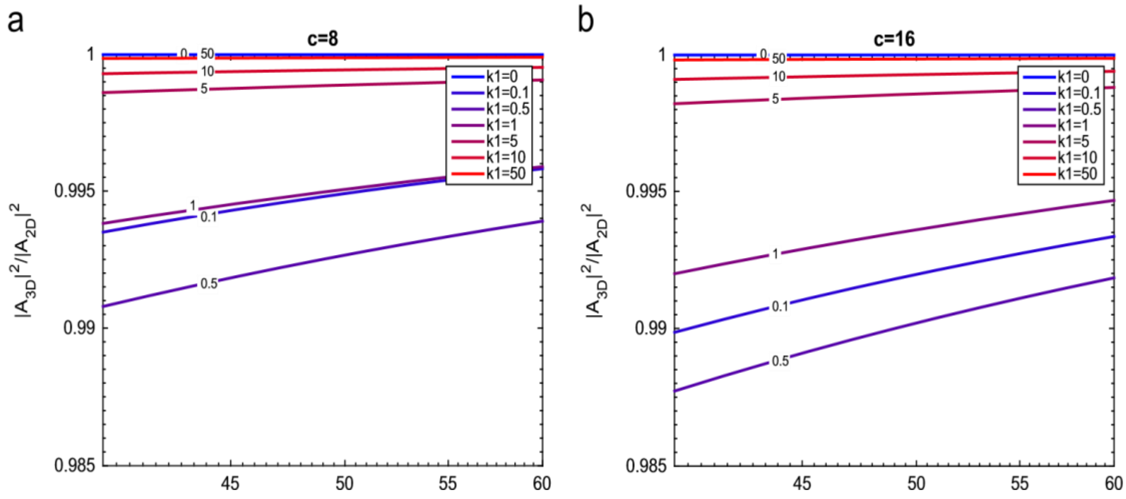

Figure 1.10: Ratio of the 2D & 3D aerodynamic admittance as a function of the aspect-ratio δ in the range typical of long-span bridges for a different reduced frequency k_1 and different correlation coefficient c. Retrieved from Reference [10].

- 2D & 3D aerodynamic admittance → *y-axis*
- Aspect ratio δ → *x-axis*

1.3 Purpose

The main objectives of this research are;

- To gain more understanding on how turbulent inflow conditions affect an aircraft at the various stages of flight (take off, climb, cruise, loiter, landing).
- To learn more about wind tunnel operations in the analysis of how gust affects an aircraft's aerodynamic properties and airframe structure.
- To gain more in-depth knowledge on aerodynamics as a subject.
- To understand the risks associated with flying in gusty conditions.
- To learn parameter and related modelling methods in the use of respective CFD software.
- To compare results obtained in this paper with those achieved and gathered by previous researchers.

1.4 Scope of Work

- Detailed study of the relevant literature related to the main topic. This includes published papers, articles, online aviation magazines and documents.
- Getting accustomed to the use and operation of CFD software such as OpenFOAM 8 to achieve the objective.

- Run CFD simulations for gust characterization for the respective conditions.
- Run CFD simulations for the lift response of 2D airfoils for the respective conditions.
- Give a detailed analysis of the gathered results.
- Give suggestions/recommendations for future work, pertaining to this field of research.
- Write a graduation thesis paper for the Degree of Bachelor of Engineering in Engineering (Aeronautical)
- Partake in a session with the relevant personnel to defend the thesis.

1.5 Paper Structure

The organizational structure of this paper is as follows:

The paper is split into different sections with the 1st being the introduction. Background information is provided on the research topic and the overall scope of the subject is fully explained and parts related to it are summarized i.e purpose, objectives etc.

The 2nd chapter of this paper provides a main focus on the theoretical aspects of the subject. Various sub-topics are studied and expanded. The literature related to the main topic is reviewed, analysed and explained. Results obtained by previous researchers are given. A foundation is laid for the following chapter in this section.

The 3rd chapter along with the following, are the main core of this thesis. The methodology of the whole investigation is given, along with further information on the steps taken to achieve the results obtained.

The 4th chapter is mainly comprised of the analysis, discussion and conclusion of the results obtained.

The 5th chapter contains the concluding remarks of this paper and information on the suggestions and proposals made for future research tasks in the specialized field of gust response, and anything else pertaining to that.

The organizational structure of this paper is sequential.

Chapter 2: THEORY

2.1 Numerical Analysis of the Functions

Theoretical Information

Equations pertaining to the relevant functions and mathematical models are given below, mainly for the transfer function, Sears function and Atassi function. In addition to this, the accompanying conditions associated with the functions are shown.

The transfer function h_L mathematical expression is shown below,

$$h_L = \frac{L_{us}}{L_{qs}} = \frac{\tilde{L}_{us}}{\tilde{L}_{qs}} e^{\emptyset i} = |h_L| e^{\emptyset i}, \tag{2.1}$$

- It is the ratio of the unsteady lift (L_{us}) (perpendicular to the average free stream) caused by the gust to the quasi-steady lift (L_{qs}) which would be produced by the steady flow at which the gust angle is equal to the angle of attack (AOA).

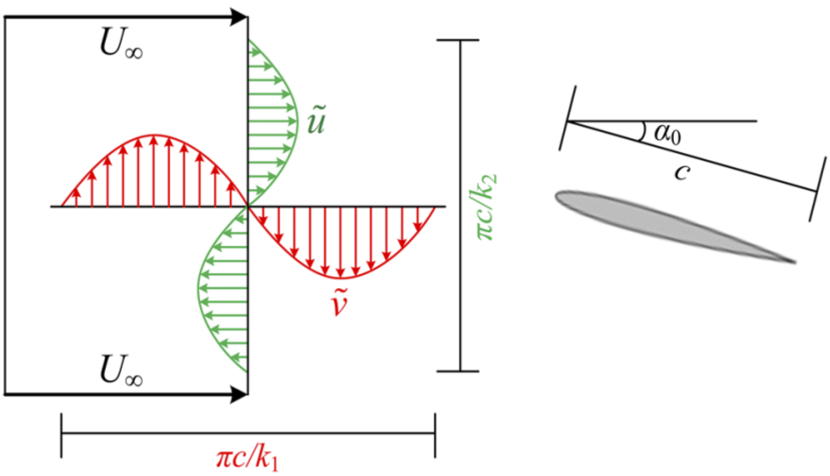

Figure 2: Image shows a test airfoil being subjected to a periodic gusty inflow condition with streamwise & vertical fluctuations. The velocity of the gust superpositions the mean free stream air velocity. (Figure from Reference [8])

In the Fig. 11 above, the respective parameters are denoted by the following symbols:

- Streamwise velocity fluctuation – u
- Vertical velocity fluctuation – v

- Mean Velocity – $U\infty$
- Amplitude of vertical velocity fluctuation - $\tilde{v}$
- Amplitude of streamwise velocity fluctuation - $\tilde{u}$

The reduced frequencies of the respective fluctuations are symbolized by, $k_1 = \pi f_1 c/U\infty$ and $k_2 = \pi f_2 c/U\infty$. The terms f_1 and f_2 denote the corresponding dimensional frequencies while c is the airfoil chord length. The installation angle is denoted by the term α_0. According to Reference [8], the condition of $k_2 = 0$ implies the streamwise velocity fluctuation ceases to exist and consequently yields the Sears problem as shown below,

$$u = U_\infty + \tilde{u}e^{2k_2 U_\infty / c(x/U_\infty - t)i}, \tag{2.2}$$

$$v = \tilde{v}e^{2k_1 U_\infty / c(x/U_\infty - t)i}, \tag{2.3}$$

Wu *et al* (2020) shows that the Atassi function can be expressed as,

$$A(k_1, k_2) = \frac{k_1}{\sqrt{k_1{}^2}} S(k_1) + \alpha A_\alpha(k_1, k_2) + \eta A_\eta(k_1, k_2), \tag{2.4}$$

The terms $A_\alpha(k_1,k_2)$ and $A_\eta(k_1,k_2)$ in equation (4) are functions of k_1 and k_2 respectively and they account for the impact of angle of attack (AOA) and airfoil camber respectively, as well. The following parameters, α and η, are the airfoil camber and angle of attack (AOA) respectively. Moreover, Wu *et al* (2020) illustrate that the gust strength can be determined by the gust angle, which is given by

$$\alpha_g = \arctan\left(\frac{v}{U_\infty + u}\right), \tag{2.5}$$

Furthermore, the following equations (2.6) & (2.7) show how the fluctuating components of gust $\tilde{L}(k_1, k_2)$, the mean component due to the mean freestream velocity $\tilde{L}(U_\infty)$, unsteady lift force L_{us}, quasi-steady lift force L_{qs}, the component due to the installation angle of the airfoil $\tilde{L}_{qs}(\alpha_0)$, the component due to gust with amplitude $\tilde{\alpha}_g$, $\tilde{L}_{qs}(\tilde{\alpha}_g)\tilde{L}_{qs}(\tilde{\alpha}_g)$, airfoil camber and thickness $\tilde{L}_{qs}(\alpha_0)$ and $\tilde{L}_{qs}(\alpha_g)$ relate to each other.

$$L_{us} = \tilde{L}_{us}(U_\infty) + \tilde{L}_{us}(k_1, k_2) = \tilde{L}_{us}(U_\infty) + \left|\tilde{L}_{us}(k_1, k_2)\right| e^{\emptyset i}, \tag{2.6}$$

$$L_{qs} = \tilde{L}_{qs}(\alpha_0) + \tilde{L}_{qs}(\tilde{\alpha}_g) = \tilde{L}_{qs}(\alpha_0) + \tilde{L}_{qs}(\tilde{\alpha}_g), \tag{2.7}$$

The magnitude of the transfer function is found by,

$$|h_L| = \frac{L_{us} - \tilde{L}_{us}(U_\infty)}{L_{qs} - \tilde{L}_{qs}(\alpha_0)}, \tag{2.8}$$

The numerical computation of this experiment was done through OpenFOAM software. Various dimensions and domains were defined the relevant protocols. The simulations were run within the incompressible Unsteady Reynolds Averaged Navier-Stokes (URANS) framework, combined with the *k*-*w* Shear Stress Transport (SST) turbulence model [8].

$$\frac{\tilde{\alpha}_g}{\tilde{\theta}} = C \tag{2.9}$$

In Eq. 2.9, the term C is a constant at an unchanged grid oscillation frequency. From this scaling law, the vane oscillation amplitude $\tilde{\theta}_{req}$ required to produce a specific gust angle $\tilde{\alpha}_g$ can be calculated using the following formula,

$$\tilde{\theta}_{req} = \frac{\tilde{\alpha}_g}{C} \tag{2.10}$$

2.2 Unsteady Lift from Inflow Turbulence

Paterson and Amiet (1977) proved the phenomenon of how airfoil thickness at high frequencies affects the unsteady lift forces that are exerted on an airfoil experiencing turbulent inflow conditions. Amiet (1975) formulated a theory on the noise produced by turbulence ingestion and the results of the former procedure were compared to the latter. Equations for the various calculations of parameters related to the unsteady lift resulting from turbulent inflow conditions are given below.

$$G_{FF}(f) = G_{vv}(f)A_{vv}(f)|H(f)|^2 b \tag{2.11}$$

$$G_{vv}(f) = 2_{U\infty}^{v^2{}_{rms}L_{11}}\left[\frac{f^2{}_e + \frac{8}{3}f^2}{f^2{}_e + f^2}\right]\left[1 + \left(\frac{f}{f_e}\right)^2\right]^{-5/6} \tag{2.12}$$

$$f_e = \frac{1}{2\sqrt{\pi}}\frac{\Gamma\left(\frac{5}{6}\right)}{\Gamma\left(\frac{1}{3}\right)}\frac{U_\infty}{L_{11}} \approx 0.12\frac{U_\infty}{L_{11}} \tag{2.13}$$

$$A_{vv}(f) = \frac{16L_{11}}{9}\left[\frac{\Gamma\left(\frac{1}{3}\right)}{\Gamma\left(\frac{5}{6}\right)}\right]^2\left[\frac{f^2}{f^2{}_e + \frac{8}{3}f^2}\right]\left[1 + \left(\frac{f}{f_e}\right)\right]^{-1/2} \tag{2.14}$$

$$|H(f)|^2 = (\pi\rho c U_\infty)^2 |S(\pi f c/U_\infty)|^2 \tag{2.15}$$

Equation (2.11): Formula to find the spectrum of the total force acting on the airfoil where $G_{vv}(f)$ is the spectral density of the turbulent velocity upstream of the airfoil, $A_{vv}(f)$ is the spanwise correlation length of the turbulent velocity, *H(f)* is the gust response function and *b* is the airfoil span.

Equation (2.12): Formula for calculating the turbulent velocity spectrum for components perpendicular to the free-stream with the term V_{rms} denoting the root mean square velocity, L_{11} being the longitudinal integral length scale of the turbulence & the characteristic frequency of the energy-containing eddies being denoted by f_e.

Equation (2.13): Formula for defining the frequency of the energy-containing eddies.

Equation (2.14): Formula for defining the spanwise correlation length of the turbulence.

- Based on the *von Karman model* [13], assuming homogeneous & isotropic turbulence, the turbulence formulae are given. Equations (2.12), (2.13) & (2.14) are based on this.
- Equation (15) is the formula for finding gust response function for a flat plate airfoil and it is derived from the two dimensional unsteady airfoil theory composed by Sears [14]. The term *S(k)* is the Sears function.

$$|S(k)|^2 \approx \left[\frac{1}{1+(2\pi k)^m}\right]^{1/m} \tag{2.16}$$

Equation (2.16) gives an approximation to $|S(k)|^2$ which is accurate to almost 0.1dB with m = 1.3. A point to note is that the gust response must be altered when the effect of airfoil thickness is factored in, [13]. A modified gust response function which includes a high frequency attenuation function and a quasi-steady correction factor is shown below,

$$|H(f)|^2 = (\pi\rho c U_\infty)^2 \left(1 + 0.8\frac{\tau}{c}\right)^2 |S(\pi f c/U_\infty)|^2 exp\left[-\beta(\tau)\frac{fc}{U_\infty}\right] \tag{2.17}$$

where,

$$\beta(\tau) \approx 0.75\,(\tau/c) + 12(\tau/c)^2 \tag{2.18}$$

Lancelot *et al* (2017) designed and tested a low subsonic wind tunnel gust generator in an attempt to investigate the possible ways in which aircraft weight can be optimised. This is due to the fact that, as time has been going by, researchers have been scouring for ways to reduce structural stresses induced by gust encounters, particularly on wing components [15]. This process was aided by the use of computational fluid dynamics (CFD).

2.3 Factors Influencing Aerodynamic Response & Lift of an Aircraft/Airfoil

Research was carried out by Commerford and Carta (1974) to analyse the unsteady response of a two-dimensional airfoil to high frequency flow changes. Results were compared with those obtained by previous researchers who had conducted similar experiments. The attenuation of the lift-factor and phase differences between aerodynamic forces & the motion creating them are visibly the most prominent effects of unsteadiness [16]. Generally, it has been seen that a great magnitude of unsteady lift results from a higher frequency. In addition to this, it is important to note that unsteady lift is caused by two primary factors, periodic changes in the horizontal and vertical flows.

Larose (1999) carried out a similar experiment but with a sole focus on a bridge deck segment. This was done to find the aerodynamic admittance (with cross-sectional admittance and spanwise distribution forces) of the examined segment and it was called the ‘segmental admittance’. It is measured by using an intrinsically two-dimensional (2D) approach and it has three-dimensional (3D) characteristics when contrasted with the cross-sectional admittance of a strip that is two dimensional (2D), [17]. Some bridge decks have aerodynamic characteristics similar to those of a thin airfoil and this property therefore makes it feasible to conduct analysis on the desired component.

$$S_{F_z}\left(f^*{}_j\right) = \left(\frac{1}{2}\rho\bar{v}B\right)^2 \left[4{C_z}^2 S_u(f^*) + {C_z}'^2 S_w(f^*)\right]|A_z(f^*)|^2 \left|J_z\left({f_j}^*\right)\right|^2 \tag{2.19}$$

Equation (2.19) is the expression for the spectrum of the modal lift forces brought up by the buffeting action of the wind on a bridge deck. The term ${f_j}^*$ is a reduced frequency equal to $f_j\, B/\bar{V}$ associated with the *j*th mode of vibration. The cross-sectional admittance of the lift is denoted by the term $|A_z(f^*)|^2$ and is linked to the vertical (w) and longitudinal (u) components of the gust. The term $\left|J_z\left({f_j}^*\right)\right|$ is the joint acceptance function of the *j*th mode. The air density, deck width, mean wind velocity at deck level, lift coefficient and the variations of the lift coefficient with angle of wind incidence are represented by the following terms: ρ, B, $\bar{V}$, C_z and ${C_z}'$. Lastly, the terms $S_{F_z,u,w}$ represent the power spectral density of the wind components *u* or *w*, or of the lift force F_z. Larose (1999) shows an approximation to the Sears function and mentions that it is a frequently used form of the aerodynamic (lift) admittance of a thin airfoil in fully correlated gusts with sinusoidal fluctuations. The function is seen in equation (2.20).

$$|\Phi_z(f^*)|^2 = \frac{1}{1+2\pi^2 f^*} \tag{2.20}$$

$$\left|J_z\left(f_j^{*}\right)\right|^2 = \int_0^l \int_0^l \frac{S_{L_1L_2}(\Delta y, f^*)}{S_L(f^*)}\ \mu_j(y_1)\mu_j\,(y_2)dy_1dy_2 \tag{2.21}$$

Equation (2.21) shows the joint acceptance function. μ_j is the *j*th mode shape while $S_{L_1L_2}/S_L$ is the normalized cross-spectrum of the lift force between strips 1 & 2 which are separated by a span-wise distance of Δy.

To gain more understanding of the concept of aerodynamic admittance and the overall scope of the subject, equations relating the two and three-dimensional aerodynamic admittance functions to the Sears strip theory and three-dimensional theory are given ahead. The formerly mentioned functions can be deduced from the latter theories, respectively.

$$|A_{3D}(k_1,\delta)|^2 = \frac{\int_{-\infty}^{+\infty} |G(k_1,k_2)|^2 \left(\frac{\sin k_2\delta}{k_2\delta}\right)^2 S_w(k_1,k_2)\,\frac{dk_2}{b}}{S_w(k_1)} \tag{2.22}$$

$$|A_{3D}(k_1,\delta)|^2 = \int_{-\infty}^{\infty} |\varkappa(k_1)|^2 \frac{k_1^2 + 2/\pi^2}{k_1^2 + k_2^2 + 2/\pi^2}\left(\frac{\sin k_2\delta}{k_2\delta}\right)^2 \frac{2ck_1b}{4\pi^2k_2^2 + c^2k_1^2}\frac{dk_2}{b} \tag{2.23}$$

$$|A_{2D}(k_1,\delta)|^2 = \int_{-\infty}^{\infty} |\chi(k_1)|^2 \left(\frac{\sin k_2\delta}{k_2\delta}\right)^2 \frac{2ck_1b}{4\pi^2k_2^2 + c^2k_1^2}\frac{dk_2}{b} \tag{2.24}$$

$$\frac{|A_{3D}(k_1,\delta)|^2}{|A_{2D}(k_1,\delta)|^2} = \frac{\int_{-\infty}^{\infty} \frac{k_1^2 + 2/\pi^2}{k_1^2 + k_2^2 + 2/\pi^2}\left(\frac{\sin k_2\delta}{k_2\delta}\right)^2 \frac{2ck_1b}{4\pi^2k_2^2 + c^2k_1^2}\frac{dk_2}{b}}{\int_{-\infty}^{\infty} \left(\frac{\sin k_2\delta}{k_2\delta}\right)^2 \frac{2ck_1b}{4\pi^2k_2^2 + c^2k_1^2}\frac{dk_2}{b}} \tag{2.25}$$

$$\lim_{\delta\to\infty} \frac{|A_{3D}(k_1,\delta)|^2}{|A_{2D}(k_1,\delta)|^2} = 1 \tag{2.26}$$

The equations above are mathematical models that explain the respective functions. The function in equation (2.22) is formed when the two wavenumber spectrum of the turbulence equation is solved simultaneously with the equation of the lift coefficient which is expressed in spectral terms [10]. The incorporation of the aspect ratio into the respective equations i.e equation for the two wavenumber spectrum of the lift coefficient, enables the derivation process for equation (2.22). The sequential process of evaluating (2.22) leads to the formation of (2.23). This is made possible by the simple process of adding the following mathematical terms, $S_w(k_{1,}k_2)$ and $G(k_1, k_2)$, into (2.22).

- Equation (2.25) serves as an expression of the ratio of the two admittance functions in (2.23) and (2.24). The sole purpose of this calculation would be to assess the disparity between the 2D strip theory and the complete 3D observation.
- Equation (2.26) is an expression in which the complexity of calculation is removed for a huge value of the span section. A bigger span section implies a larger aspect ratio and therefore, the two and three dimensional admittances are equalised.

The content of this section pertains to the theoretical aspects of the background knowledge given in the 1st chapter. The various expressions provided are there to aid one's understanding of the Atassi function, Sears function, Unsteady Lift and aerodynamic admittance. The terms in the expressions are defined. Moreover, brief explanations are given on how they relate to each other and how they fit into the overall scope of studying the mathematical models of the inflow conditions.

Chapter 3: NUMERICAL METHODOLOGY

This section of the paper documents the process carried out to produce the results of the analysis, of which will be discussed further forward. The simulations performed over the course of this research were run using OpenFOAM 8™ software. This software is part of the Computational Fluid Dynamics (CFD) package and it is open source, a feature which contributes to its ease of use. Previous researchers have used this software to provide proof of results and knowledge to supplement their work. Despite its difficulty of being hard to learn and grasp, it is an open source software and therefore makes it slightly better in that regard, compared to other CFD programs.

As an imperative task for this investigation, three test cases were run and analysed. The first 2 cases were for *'Atassi Gust'*. The 3 overall simulations were for 'Wing Motion 2D Gust Angle 2'. The velocity for case 1 & 2 was U=25 with a frequency of 5 & 8 respectively. The third case was for *'Sears Gust'* with a velocity of U=20 and frequency value of 8.

3.1 Numerical Computation

The simulation type used in all three cases is the Reynolds-Averaged Simulation (RAS) and this can be seen within the 'turbulenceProperties' file of each case. The solver used for all the three cases was 'pimpleFoam'. It is a combined algorithm of the 'PISO' and 'SIMPLE' algorithms and is used for transient problems such as the ones in this paper.

3.1.1 Governing Equations

The equations in the first part of this sub-section are the governing equations for fluids and their flow. These are the momentum equation and continuity equation. In fluid continuum mechanics, the format by which the equations are written, in a three-dimensional system is given below [18].

Mass conservation equation,

$$\frac{\partial \rho}{\partial t} + \nabla \cdot (\rho \mathbf{u}) = 0 \tag{3.1}$$

Conservation of momentum,

$$\frac{\partial\rho\mathbf{u}}{\partial t}+\nabla\cdot(\rho\mathbf{uu})=\rho\mathbf{g}+\nabla\cdot\sigma \tag{3.2}$$

Conservation of energy,

$$\frac{\partial\rho e}{\partial t}+\nabla\cdot(\rho e\mathbf{u})=\rho\mathbf{gu}+\nabla\cdot(\sigma\mathbf{u})-\nabla\cdot\mathbf{q}+\rho Q \tag{3.3}$$

In the equations above, **σ** is the shear stress tensor, **e** is the total specific energy, **ρ** is the density of the fluid, **Q** is the volume energy source, **u** is the 3D velocity field, **g** is the vector of the acceleration due to gravity and **q** is the heat flux.

$$\nabla\cdot\mathbf{u}=0 \tag{3.4}$$

$$\frac{\partial\mathbf{u}}{\partial t}+\nabla\cdot(\mathbf{uu})=\mathbf{g}-\nabla p+\nabla\cdot(\upsilon\nabla\mathbf{u}) \tag{3.5}$$

Equation (3.4) is a simplified form of equations (3.1), (3.2) and (3.3) for any incompressible and isothermal Newtonian fluid. It is basically the simplification of the mass conservation equation. υ is the kinematic viscosity while p is the kinematic pressure in equation (3.5).

The running of the simulations was assigned to four processors using parallel computation. The `decomposePar` command was run inorder for this to happen. After this process, the split mesh was reconstructed into an integral one using the `reconstructPar` command. The final command used was for viewing the simulated case in the graphical application, ParaView, using the `paraFoam` or `paraview foam.foam` commands.

The concise sequential input of the commands is given below,

1. `cd $HOME/Thesis` → `openfoam8-macos -p`
2. `cd $FOAM_RUN` → `cd ‘case name’`
3. `decomposePar`
4. `mpirun -np 4 pimpleFoam -parallel > log/log&`: parallel simpleFoam steady computation in the background.
5. `reconstructPar`

6. `paraFoam` or `paraview foam.foam`

In step 4, the term '`-np 4`' indicates the number of blocks/processors the mesh will split into for processing. As mentioned above, the solver used for the cases in this paper is pimpleFoam. Lastly, the term '`-parallel > log/log`' is for ensuring that the parallel computation of the process will be initiated, with '`&`' making the simulation process to happen in the background (optional). The first step contains commands typed into the terminal for opening OpenFOAM 8 in the system and accessing the case from within the case directory.

3.1.2 Finite Volume Method (FVM)

Discretization Schemes

- The *Time discretization scheme* used for the 3 cases was **Euler**, which is a time dependant and 1st order scheme. First order means that it is bounded and stable.
- The *Gradient discretization scheme* used for the 3 cases was **Gauss linear**.
- The *Laplacian terms discretization* used for the 3 cases was **corrected**, which is used for meshes with non-orthogonality & grading.
- Lastly, the *Convective terms discretization* schemes for the 3 cases were Gauss **linearUpwind** grad(U) for div(phi,U), Gauss **limitedLinear** 1 for div(phi,k), Gauss **limitedLinear** 1 for div(phi,omega) and Gauss **linear** for div((nuEff*dev2(T(grad(U))))).
- For verification and confirmation purposes, reference can be made to the *fvSchemes* files in **Appendix A** ahead.

The Finite Volume Method (FVM) has no need of a structured mesh for calculations and computations thereby making it advantageous to use over other methods. A key concept to be applied in analysing and understanding the Finite Volume Method (FVM) is the divergence theorem, also known as Gauss theorem [19]. It is used to convert the volume integrals in the governing equations to surface integrals. The Gauss theorem is given below.

$$\int_V \nabla \cdot \mathbf{a} dV = \oint_{\partial V} d\mathbf{S} \cdot a \tag{3.6}$$

The equation given below is known as the generic transport equation,

$$\int_{V_P} \frac{\partial \rho \phi}{\partial t} dV + \sum_f \mathbf{S}_f \cdot (\rho \mathbf{u} \phi)_f - \sum_f \mathbf{S}_f \cdot \left(\rho \Gamma_\phi \nabla \phi\right)_f = \left(S_c V_P + S_p V_{P\phi P}\right) \tag{3.7}$$

where ρ is the density, Γ is the diffusivity and **u** is the velocity field. It must be noted that ϕ is a generic scalar. The terms in the generic transport equation above are defined as,

- Temporal Derivative → $\frac{\partial \rho \phi}{\partial t} dV$
- Convective Flux → $S_f \cdot (\rho u \phi)_f$
- Diffusive Flux → $S_f \cdot \left(\rho \Gamma_\phi \nabla \phi\right)_f$
- Source Term → $\left(S_c V_P + S_p V_{P\phi P}\right)$

The discretization of equation (3.2) over a time interval of *t* to *t*+Δ*t* produces equation (3.8) below.

$$\int_t^{t+\Delta t} \left[\left(\frac{\partial \rho \phi}{\partial t} \right)_P V_P + \sum_f S_f \cdot (\rho u \phi)_f - \sum_f S_f \cdot \left(\rho \Gamma_\phi \nabla \phi \right)_f \right] dt = \int_t^{t+\Delta t} \left(S_c V_P + S_p V_{P\phi P} \right) dt \tag{3.8}$$

Chapter 4: Results Analysis & Discussion

4.1 Cases & Results

4.1.1 Wing Motion (2D)/pimpleFoam/Gust Angle 2°/U25/f5 (*Atassi Inflow Conditions*)

- *For the following figures, it must be noted that* ***1 period (T) = 0.2s****.*

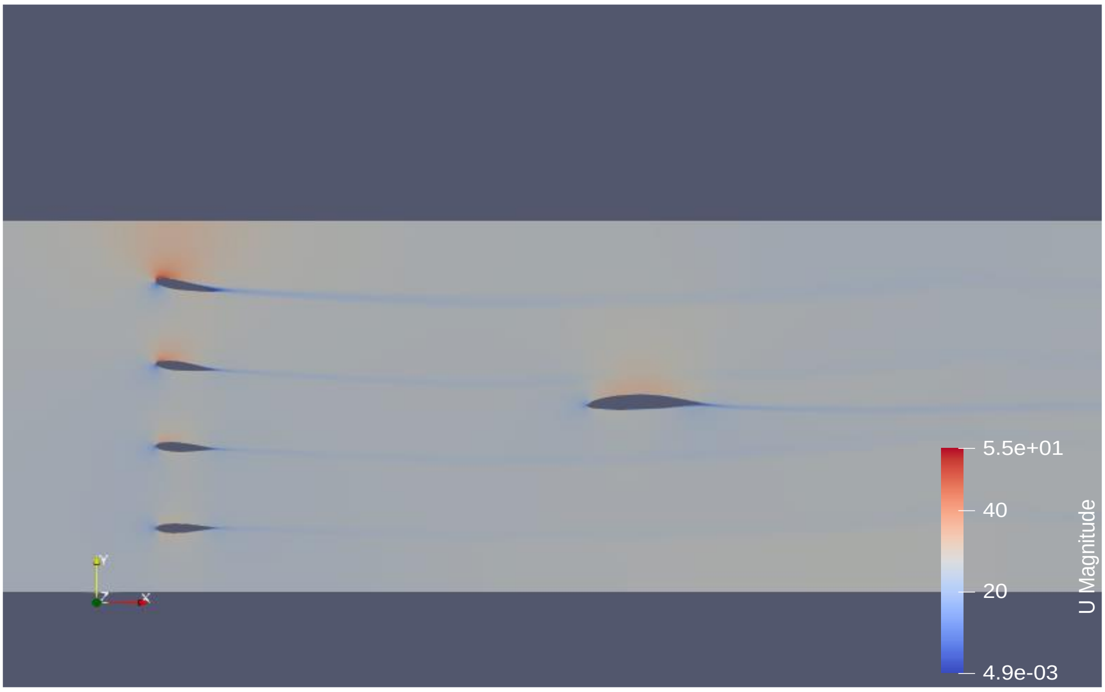

Figure 4.1(a): Velocity magnitude profile for the Atassi gusty inflow at t/T = 1/8, together with the flow field of the freestream velocity (U_{∞} = 25m/s), frequency f = 5Hz and gust angle α_g = 2°.

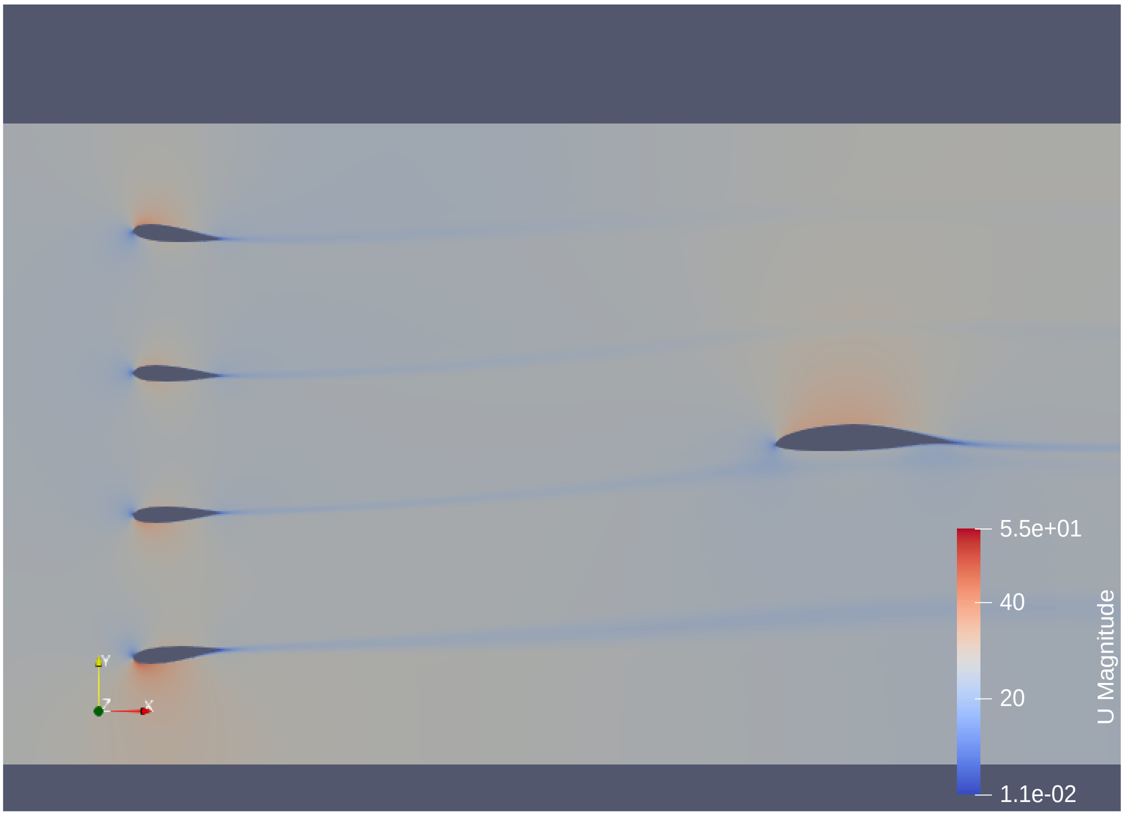

Figure 4.1(b): At t/T = 1/4. Image shows position of the oscillating vanes halfway through the first oscillation. The vanes take a more linear shape across the horizontal axis hence showing movement from the initial angle position in Fig. 4.1(a) above.

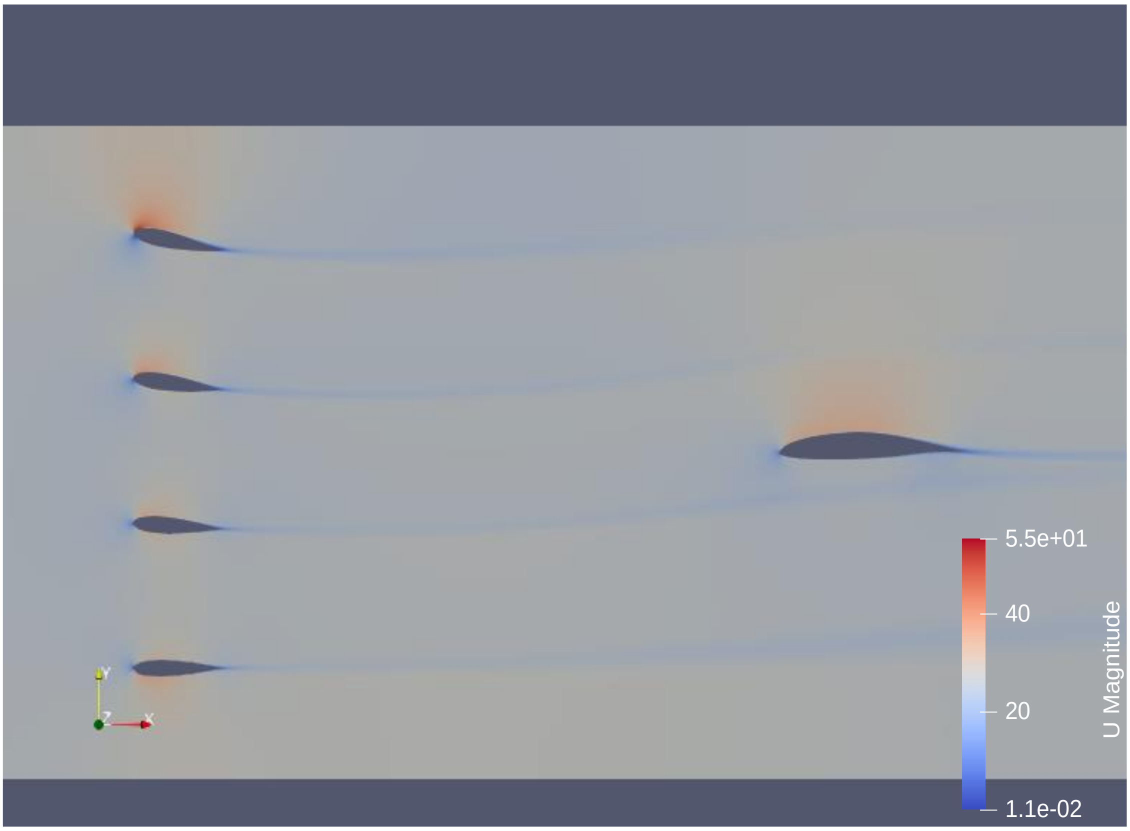

Figure 4.1(c): The focused protocol for the Atassi inflow at t/T = 3/8, together with the flow field of the freestream velocity (U_∞ = 25m/s), frequency f = 5Hz and gust angle α_g = 2°.

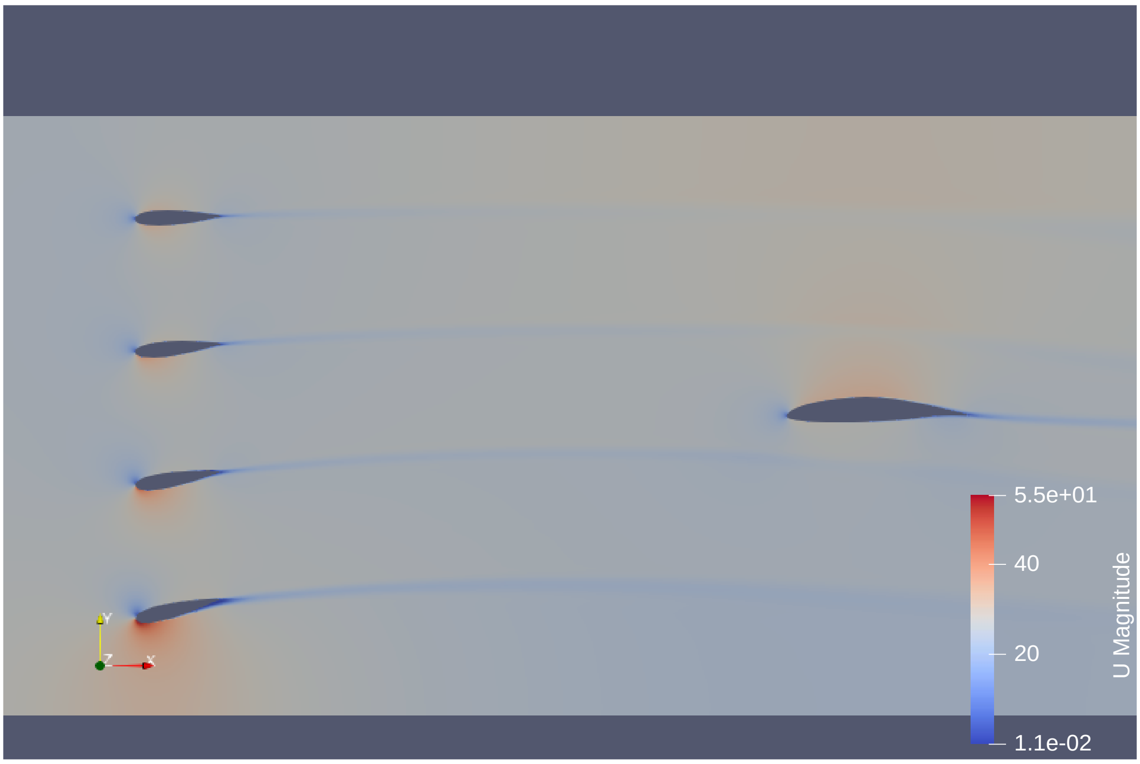

Figure 4.1(d): The positional structure of the oscillating vanes at t/T = 1/2. The velocity flow field is shown for the same parameters as those shown in Fig. 4.1(a) above.

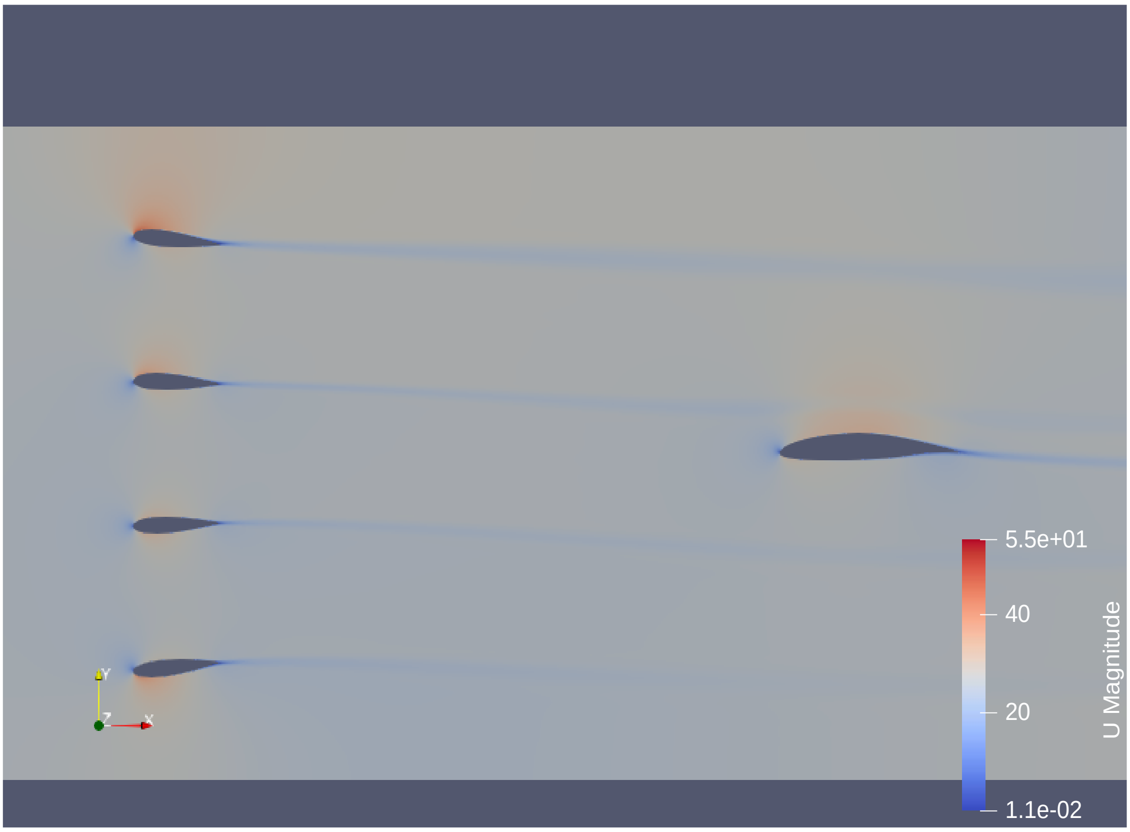

Figure 4.1(e): The positional structure of the oscillating vanes at t/T=5/8. The velocity flow field is shown for the same parameters as those shown in Fig. 4.1(a) above.

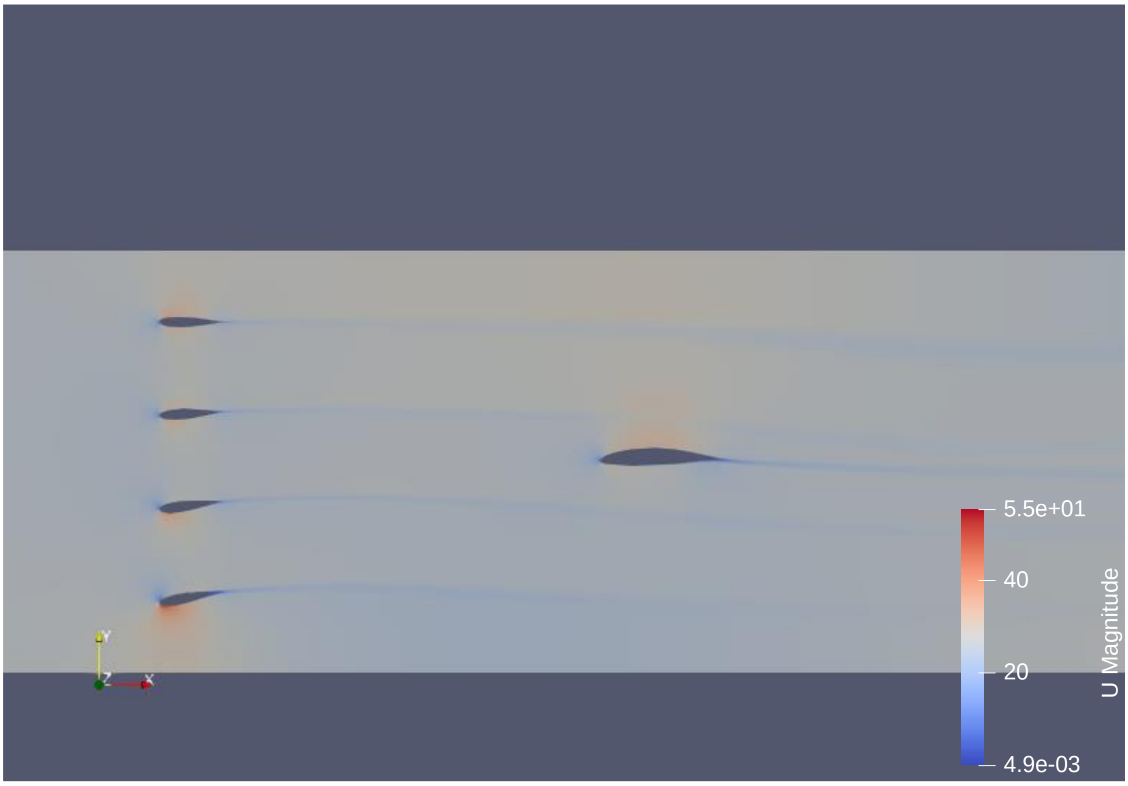

Figure 4.1(f): The positional structure of the oscillating vanes at t/T=3/4. The velocity flow field is shown for the same parameters as those shown in Fig. 4.1(a) above.

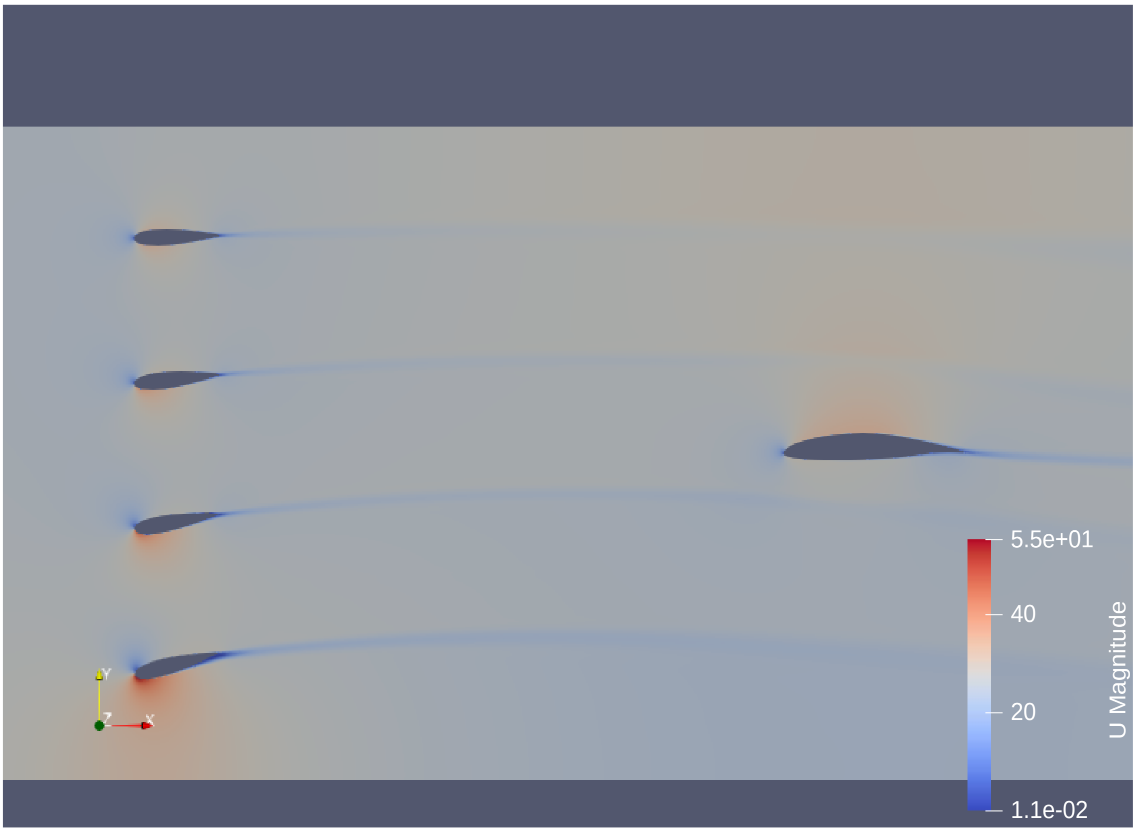

Figure 4.1(g): The positional structure of the oscillating vanes at t/T=7/8. The velocity flow field is shown for the same parameters as those shown in Fig. 4.1(a) above. Fourth vane from the top shows a high pressure point at the leading edge which yields an increase in the velocity.

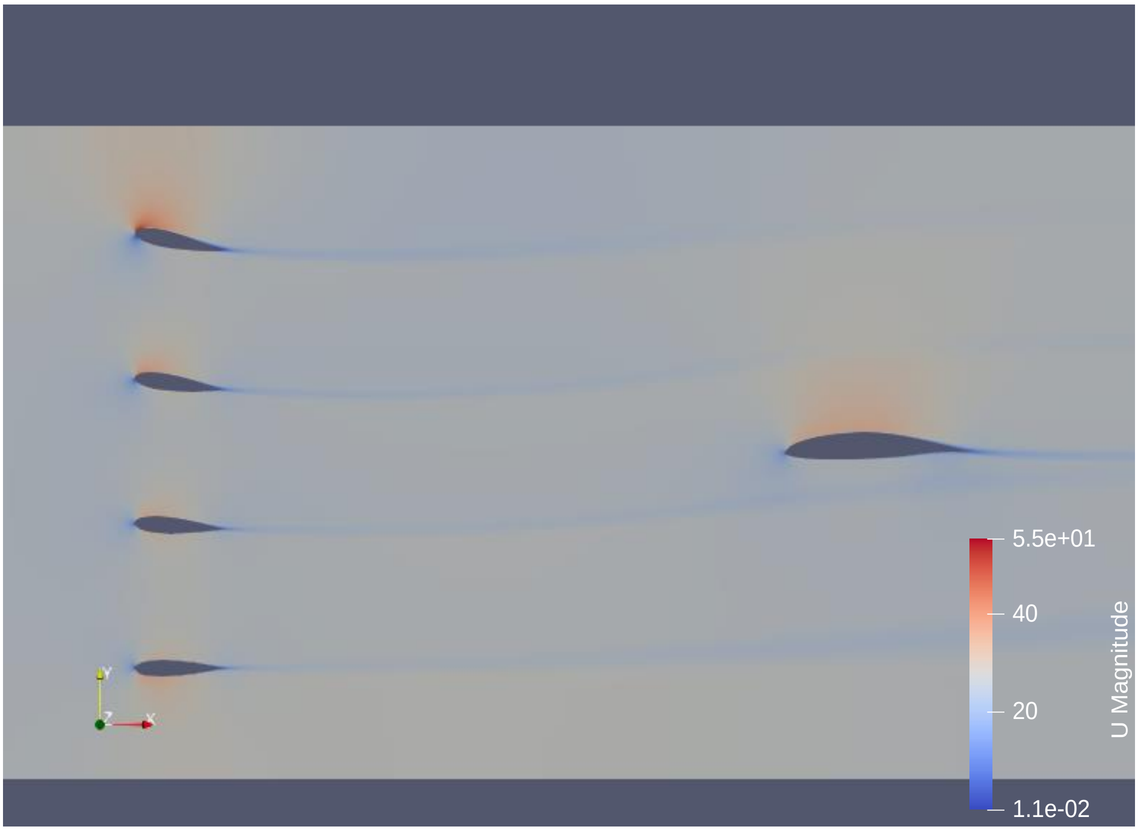

Figure 4.1(h): The positional structure of the oscillating vanes at t/T=1. The velocity flow field is shown for the same parameters as those shown in Fig. 4.1(a) above. Deflection of oscillating vanes results in an increase in the magnitude of the velocity at the leading edge of the top/first vane.

Streamlines

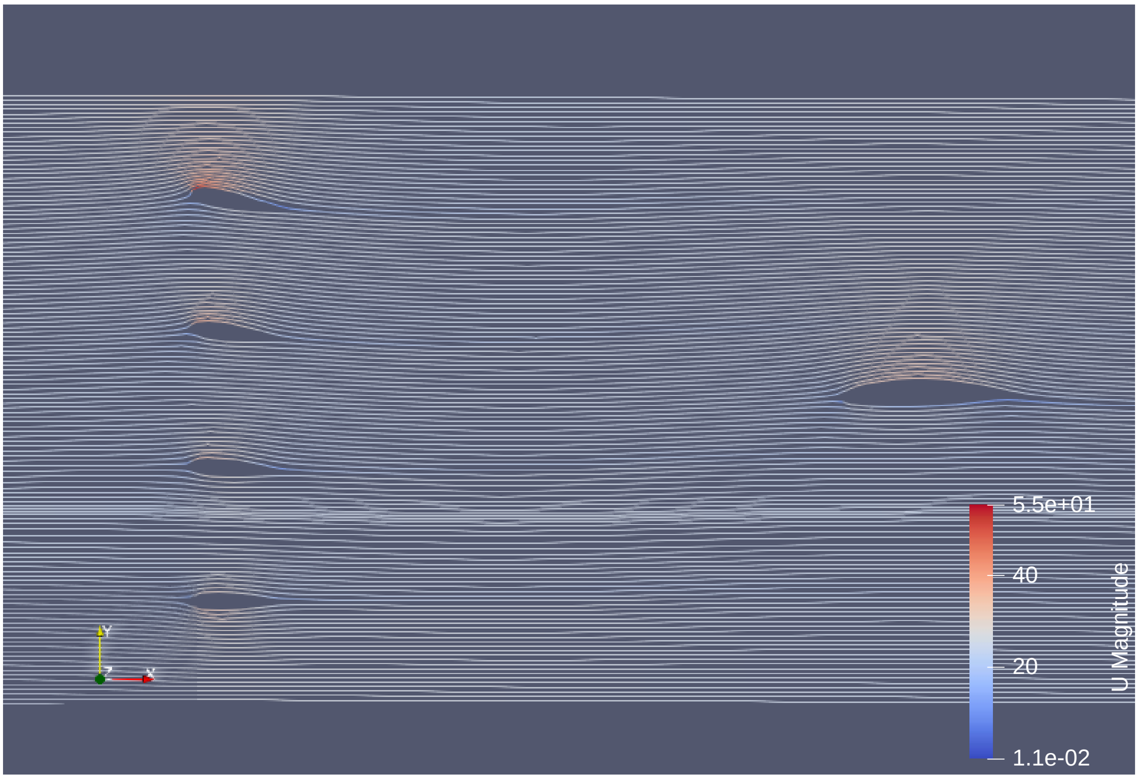

Figure 4.2(a): Average trajectory of the streamlines of the velocity flow field when the 4 oscillating vanes rotate through an angle of 2° upward from the position in Fig. 4.2(b) below for focused protocol (Case 1) with frequency, f = 5Hz.

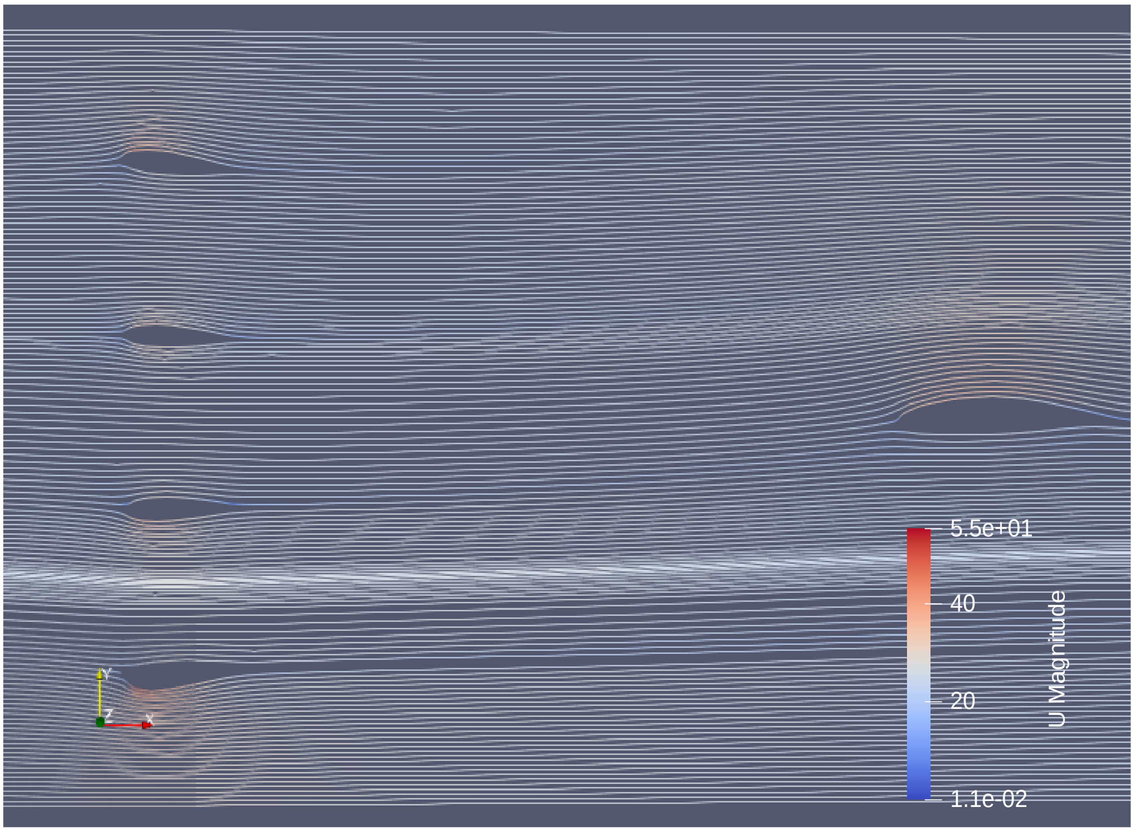

Figure 4.2(b): Average trajectory of the streamlines of the velocity flow field when the 4 vanes maintain a similar flat, horizontal position after deflection, for focused protocol (Case 1) with frequency, f = 5Hz.

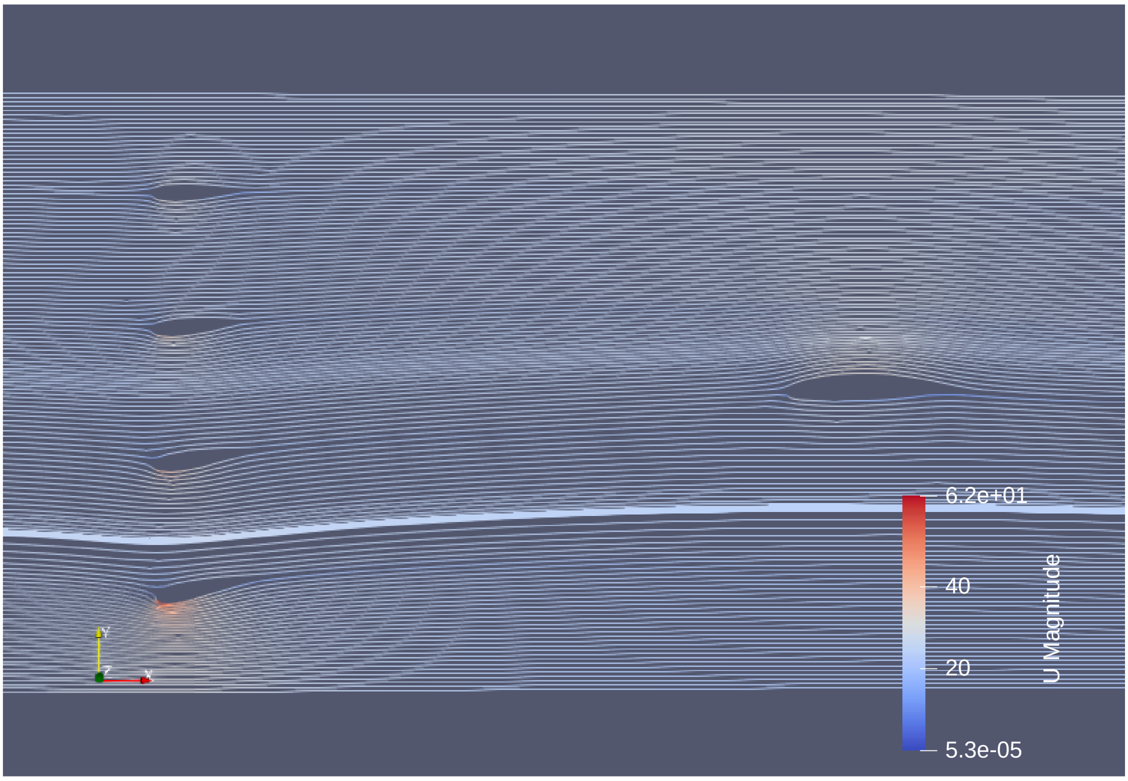

Figure 4.2(c): Average trajectory of the streamlines of the velocity flow field when the 4 oscillating vanes rotate through an angle of 2° downward from the position in Fig. 4.2(b) for focused protocol (Case 1) with frequency, f = 5Hz.

4.1.2 Wing Motion (2D)/pimpleFoam/Gust Angle 2°/U25/f8 (*Atassi Inflow Conditions*)

- *For the following figures, it must be noted that* ***1 period (T) = 0.125s.***

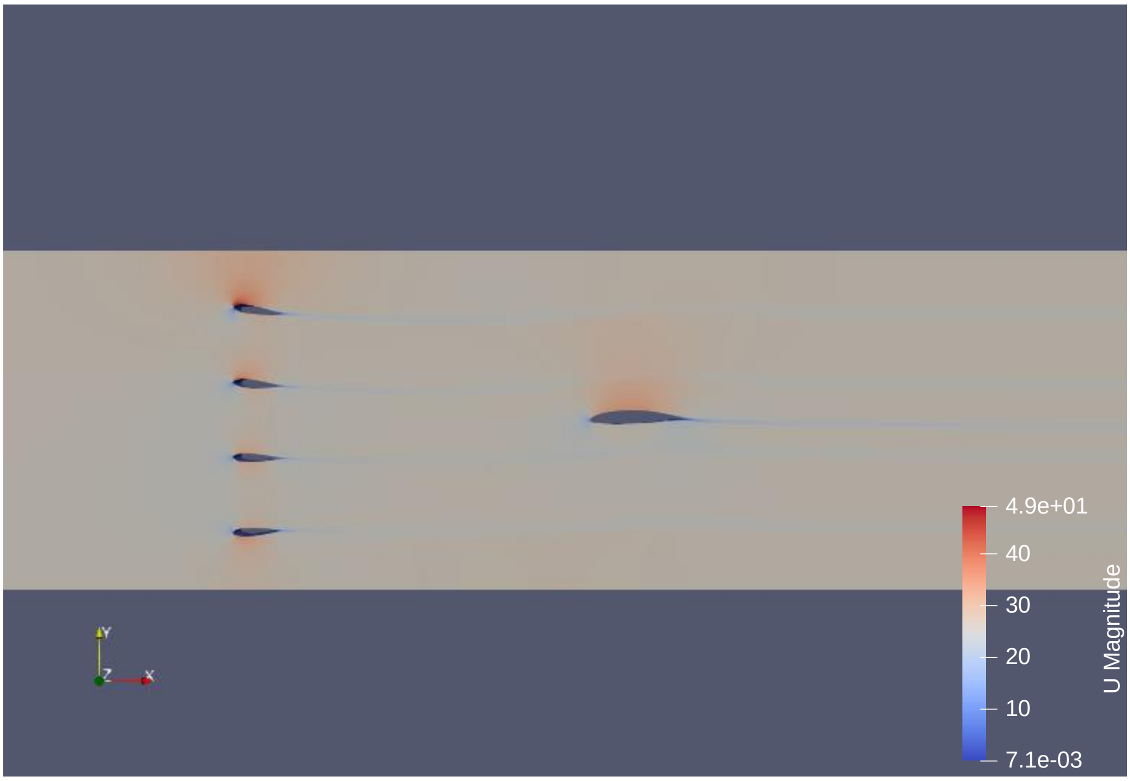

Figure 4.3(a): Velocity magnitude profile for the Atassi gusty inflow at the start of one oscillation period, t/T=0, together with the flow field of the freestream velocity (U_∞ = 25m/s), frequency f = 8Hz and gust angle α_g = 2°.

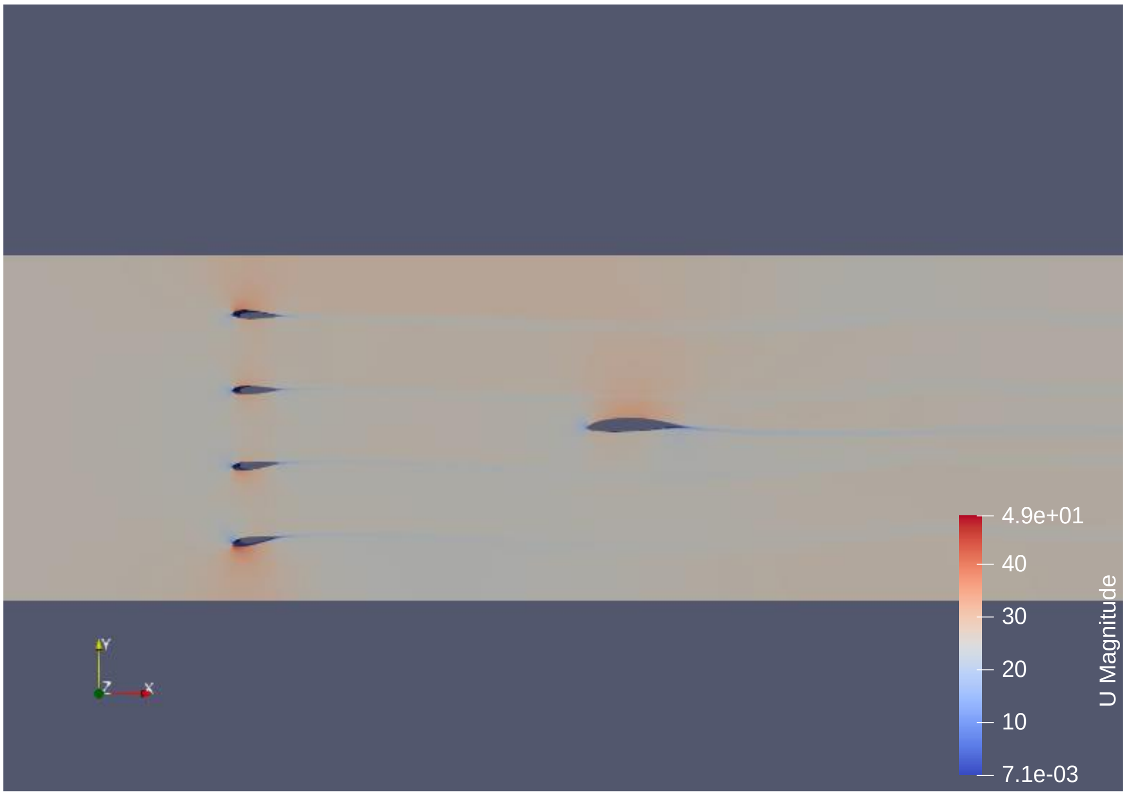

Figure 4.3(b): Velocity magnitude profile for the Atassi gusty inflow at the start of one oscillation period, t/T=1/5, together with the flow field of the freestream velocity (U_∞ = 25m/s), frequency f = 8Hz and gust angle α_g = 2°.

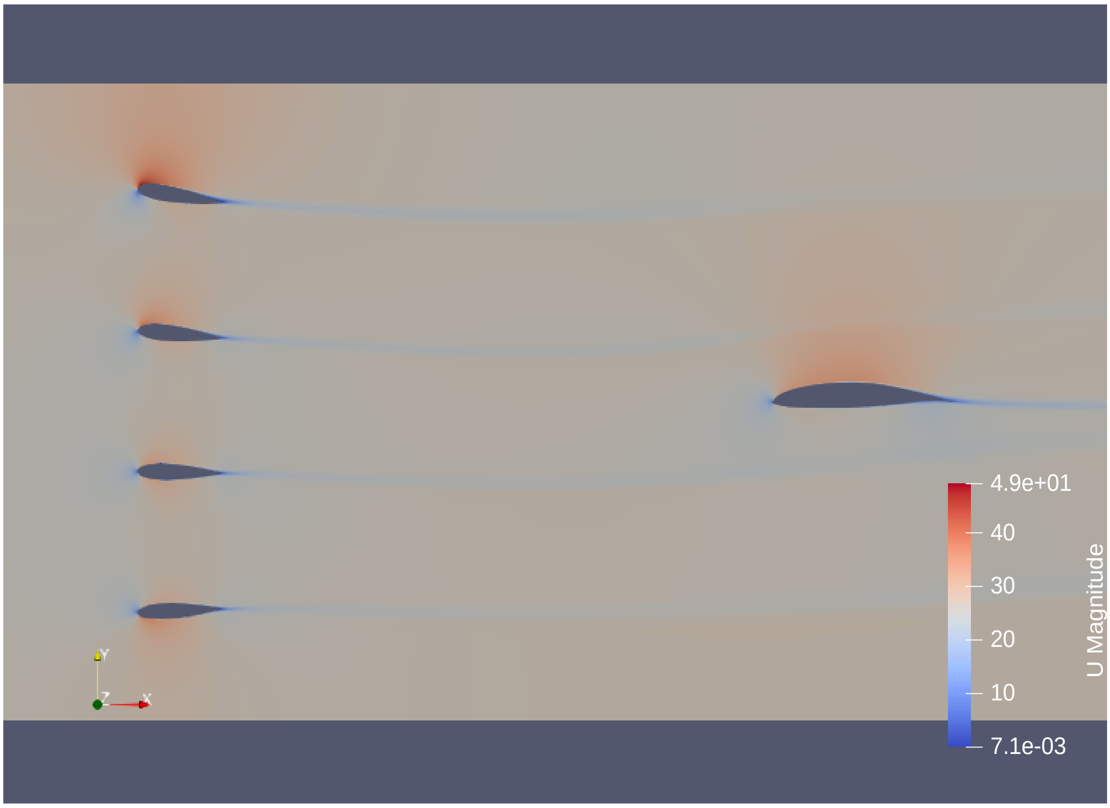

Figure 4.3(c): Velocity magnitude profile for the Atassi gusty inflow at the start of one oscillation period, t/T=2/5, together with the flow field of the freestream velocity (U_∞ = 25m/s), frequency f = 8Hz and gust angle α_g = 2°. Velocity flow field is shown along with the position of the oscillating vanes.

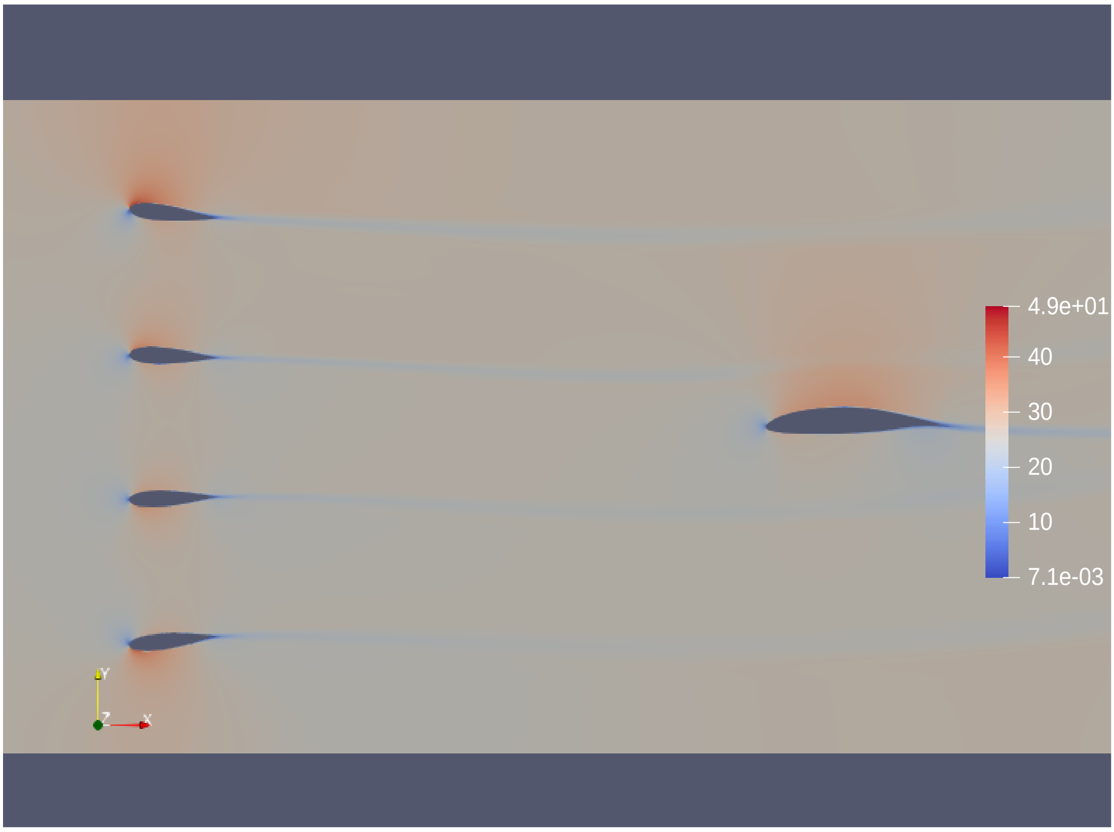

Figure 4.3(d): Velocity magnitude profile for the Atassi gusty inflow at the start of one oscillation period, t/T=3/5, together with the flow field of the freestream velocity (U_∞ = 25m/s), frequency f = 8Hz and gust angle α_g = 2°.

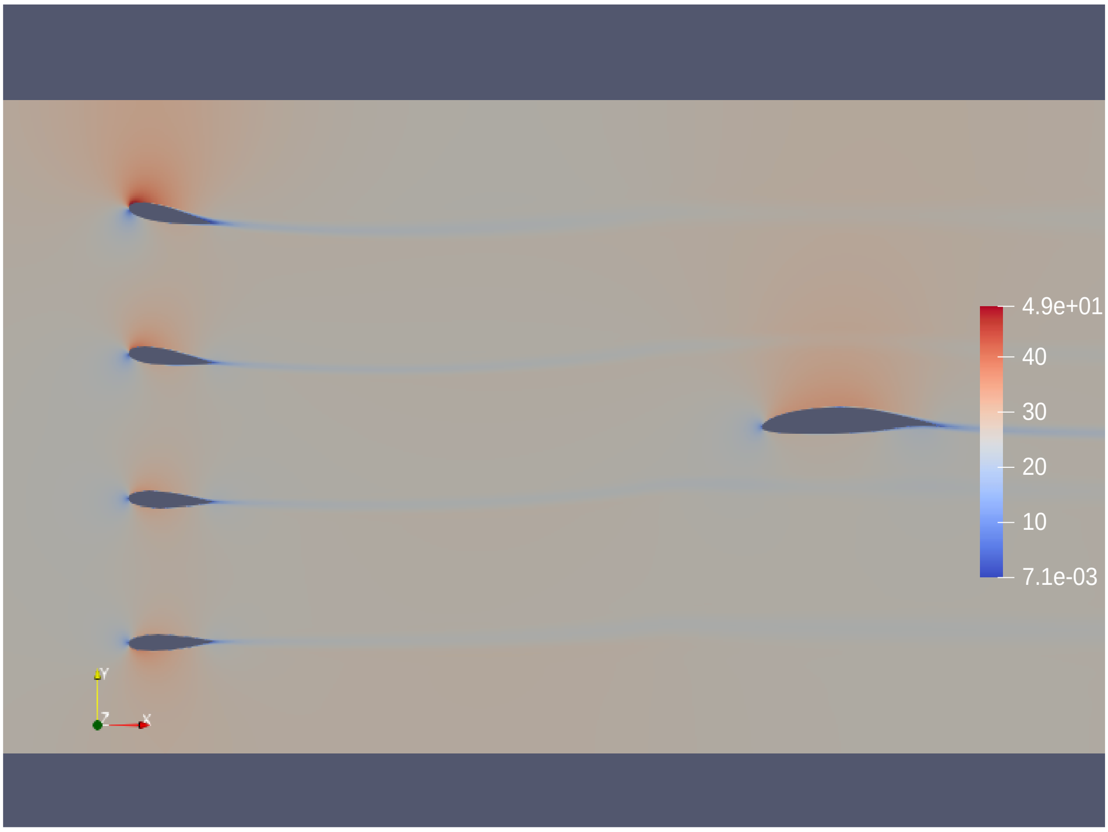

Figure 4.3(e): Velocity magnitude profile for the Atassi gusty inflow at the start of one oscillation period, t/T=4/5, together with the flow field of the freestream velocity (U_∞ = 25m/s), frequency f = 8Hz and gust angle α_g = 2°.

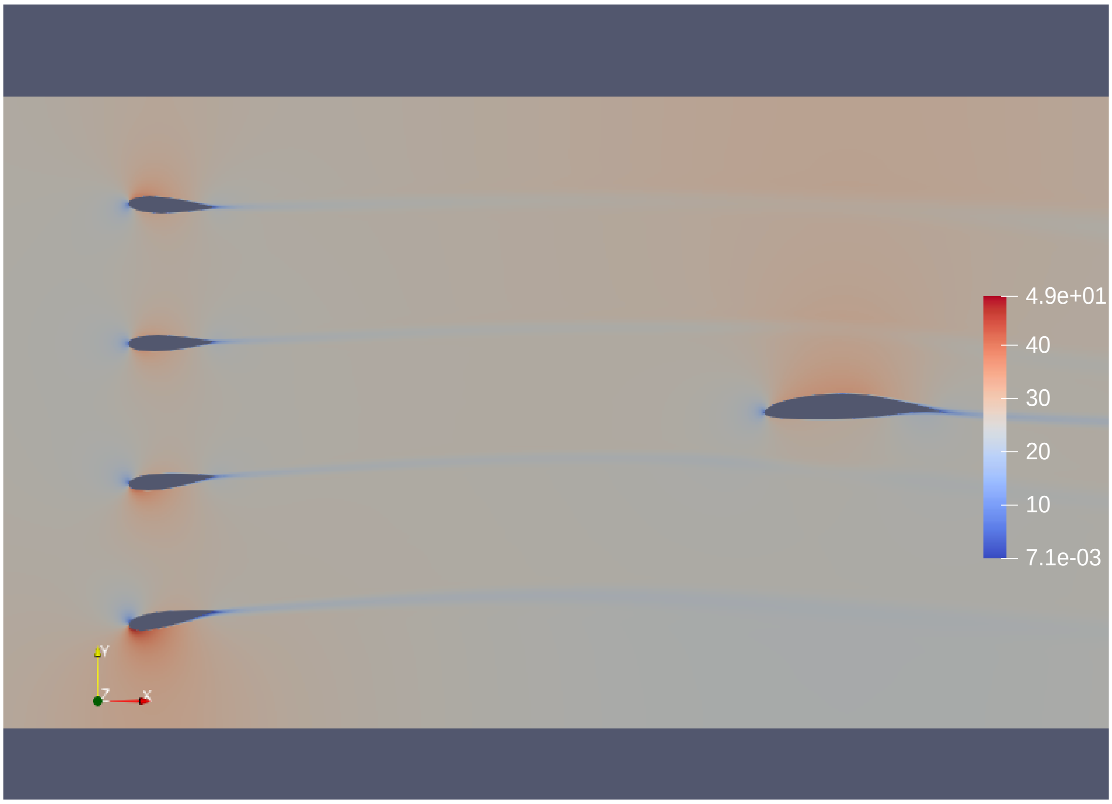

Figure 4.3(f): Velocity magnitude profile for the Atassi gusty inflow at the start of one oscillation period, t/T=1, together with the flow field of the freestream velocity (U_∞ = 25m/s), frequency f = 8Hz and gust angle α_g = 2°.

Streamlines

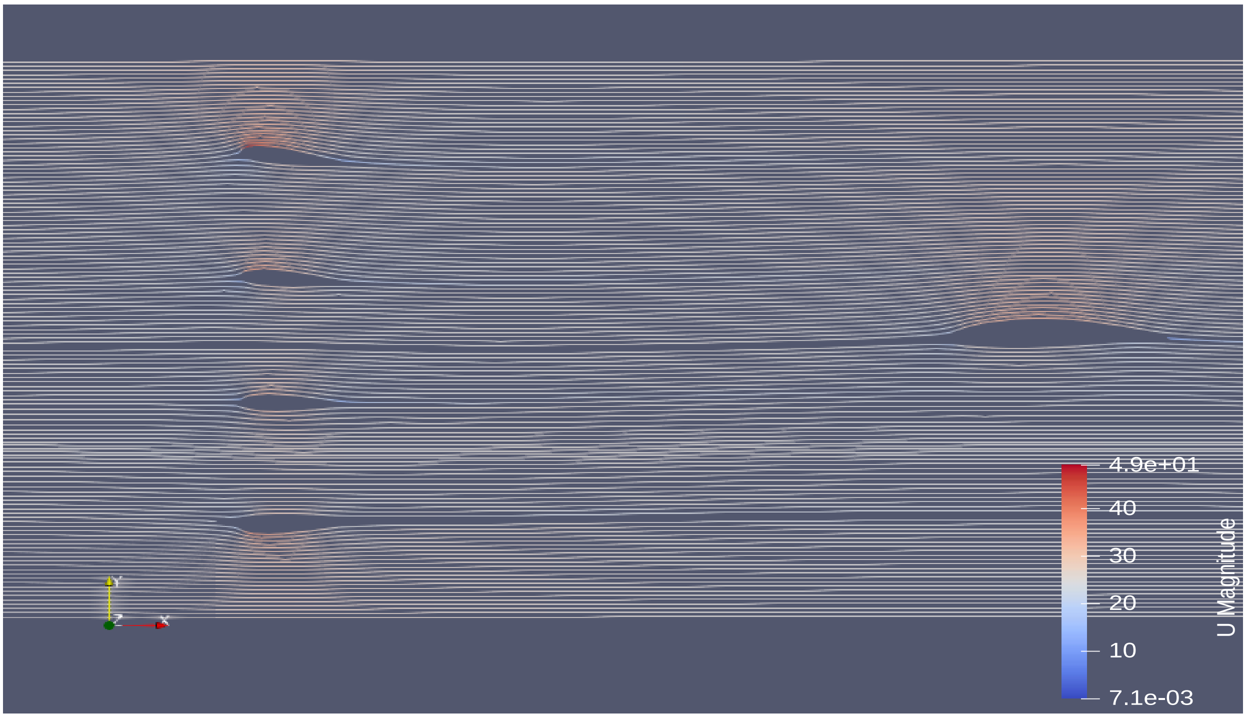

Figure 4.4(a): Average trajectory of the streamlines of the flow field with respect to freestream velocity, U_∞, at a first instance for focused protocol (Case 2) with frequency, f = 8Hz.

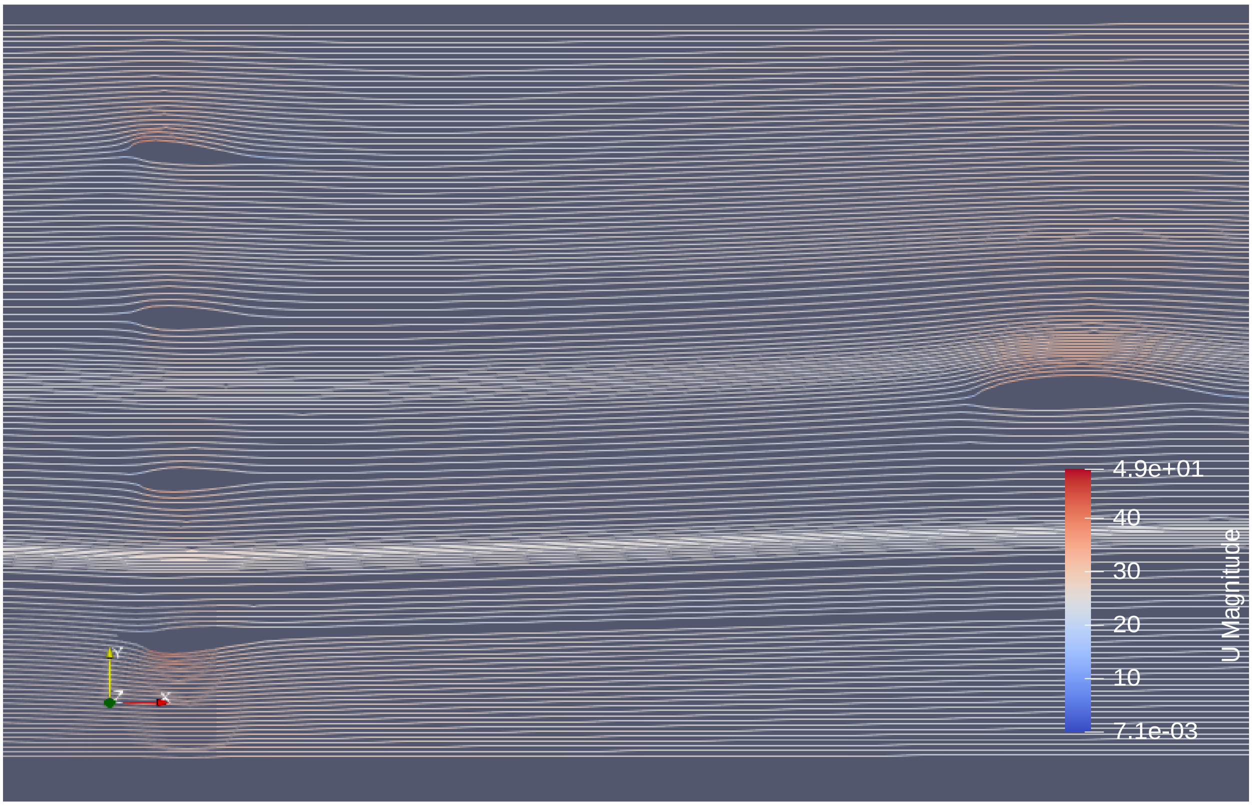

Figure 4.4(b): Average trajectory of the streamlines of the flow field with respect to freestream velocity, U_∞ at a second instance for focused protocol (Case 2) with frequency, f = 8Hz.

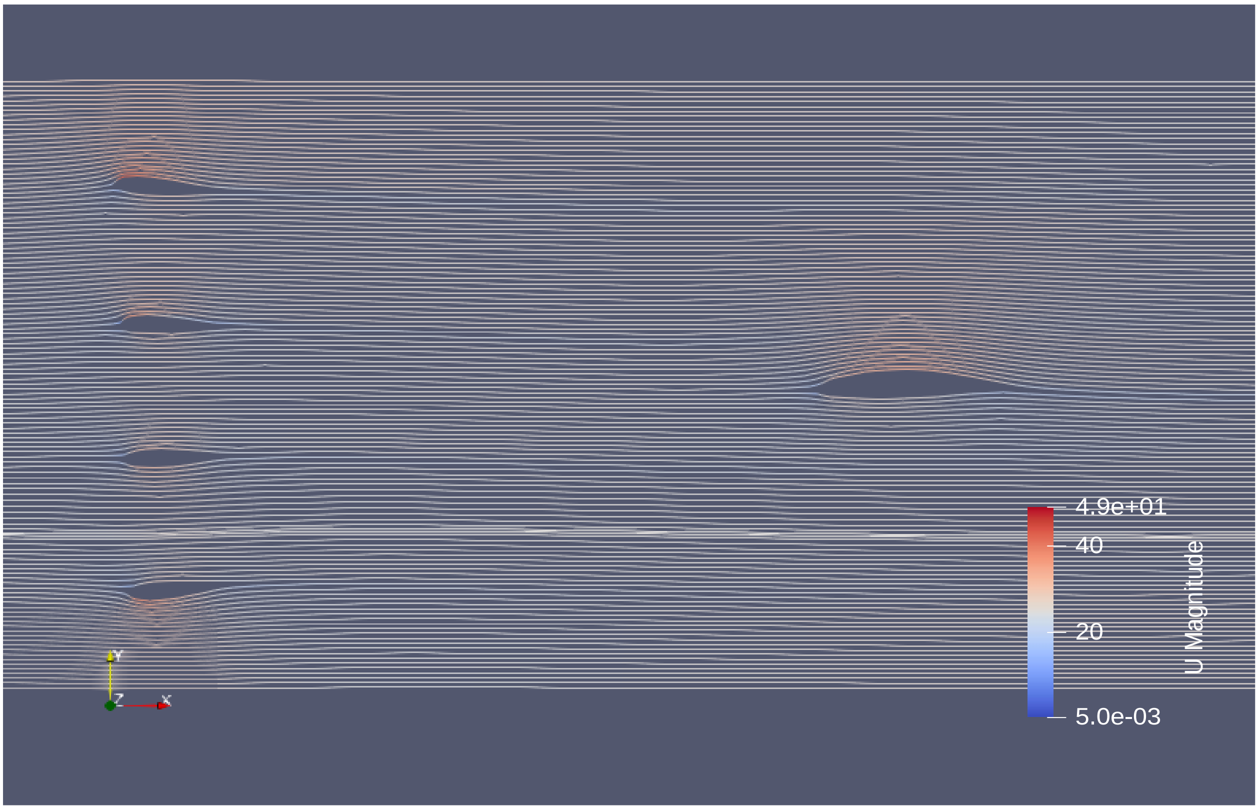

Figure 4.4(c): Average trajectory of the streamlines of the flow field with respect to freestream velocity, U_∞, at a third instance for focused protocol (Case 2) with frequency, f = 8Hz.

4.1.3 Wing Motion (2D)/pimpleFoam/Gust Angle 2°/U20/f8 (*Sears Inflow Conditions*)

Figure 4.5(a): Velocity magnitude profile for the Sears gusty inflow at t/T = 0, together with the flow field of the freestream velocity (U_∞ = 20m/s), frequency f = 8Hz and gust angle α_g = 2°.

Figure 4.5(b): Velocity magnitude profile for the Sears gusty inflow at t/T = 1/2, together with the flow field of the freestream velocity (U_∞ = 20m/s), frequency f = 8Hz and gust angle α_g = 2°.

Streamlines

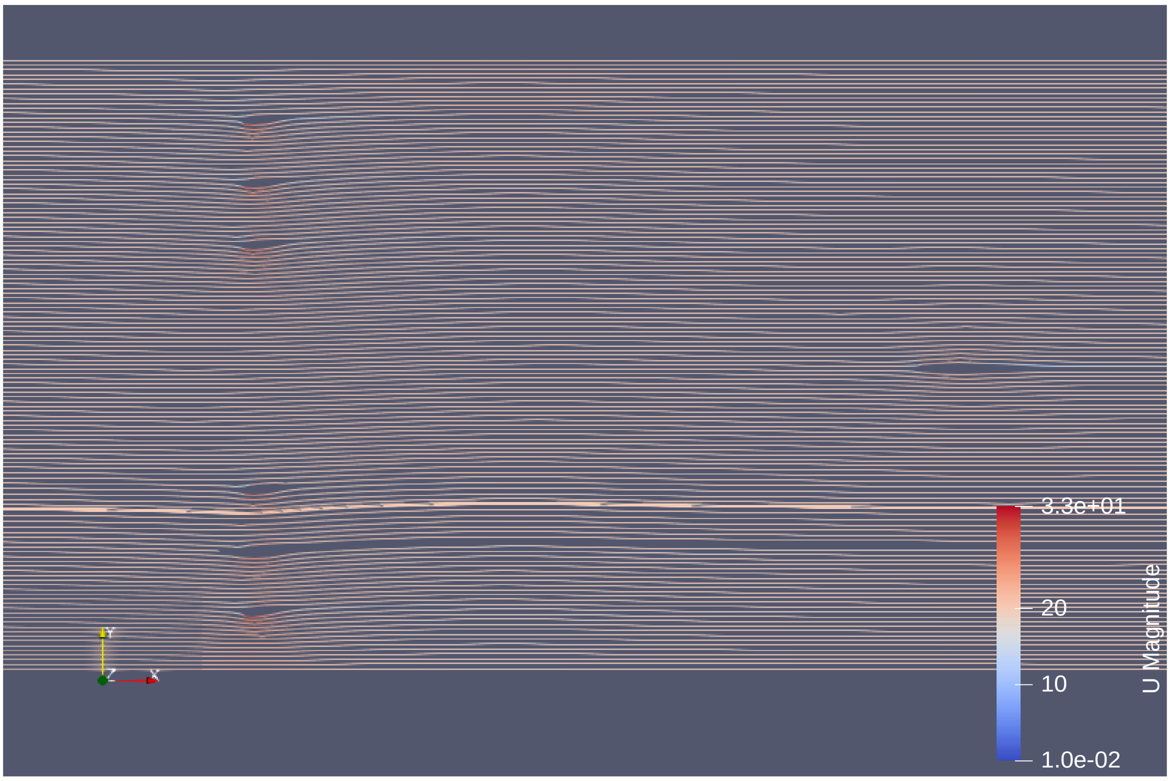

Figure 4.6: Average path of the streamlines of the flow field with respect to freestream velocity, U_∞, for limited protocol (Case 3) with frequency, f = 8Hz.

- It must be noted that the frequency of the Sears inflow conditions in Fig. 4.5(a) and (b) is determined by the frequency of the six oscillating vanes. In these figures, the velocity flow field is shown for a period (T) of 0.125s. The position of the oscillating vanes halfway through oscillation of period T = 0.2s and T = 0.125s are illustrated in the relevant figures above for the Atassi gusty inflow with frequencies f = 5Hz and f = 8Hz respectively, as seen in the captions. The streamlines of the Sears gusty inflow are visualised in Fig. 4.6 and by analysing the relatively laminar flow, it can be deduced that the structure of the Sears gusty inflow is determined by the turbulent wakes of the oscillating vanes. This is a basic theory which is explained further in the following section by means of elaboration on the aerodynamic coefficient curves obtained from the numerical computation and simulation of the cases. There is not much deviation between the results in this paper for the periodic vane oscillations for the Atassi inflow conditions in Fig. 4.1(a) to (h) and Fig. 4.3(a) to (f), and those achieved by Wu *et al* (2020). The streamlines for the Atassi inflow conditions in Fig. 4.2(a) to (c) and Fig. 4.4(a) to (c) represent the velocity flow field and, the absence of turbulent flow is evident. The darkened crimson colour sections symbolize the zones in which the velocity (*U*) of the gusty inflow is heightened. Conversely, they also represent zones of high pressure (*p*).

4.2 Graphed Results of Aerodynamic Coefficients (C_m, C_d, C_L)

Case 1.

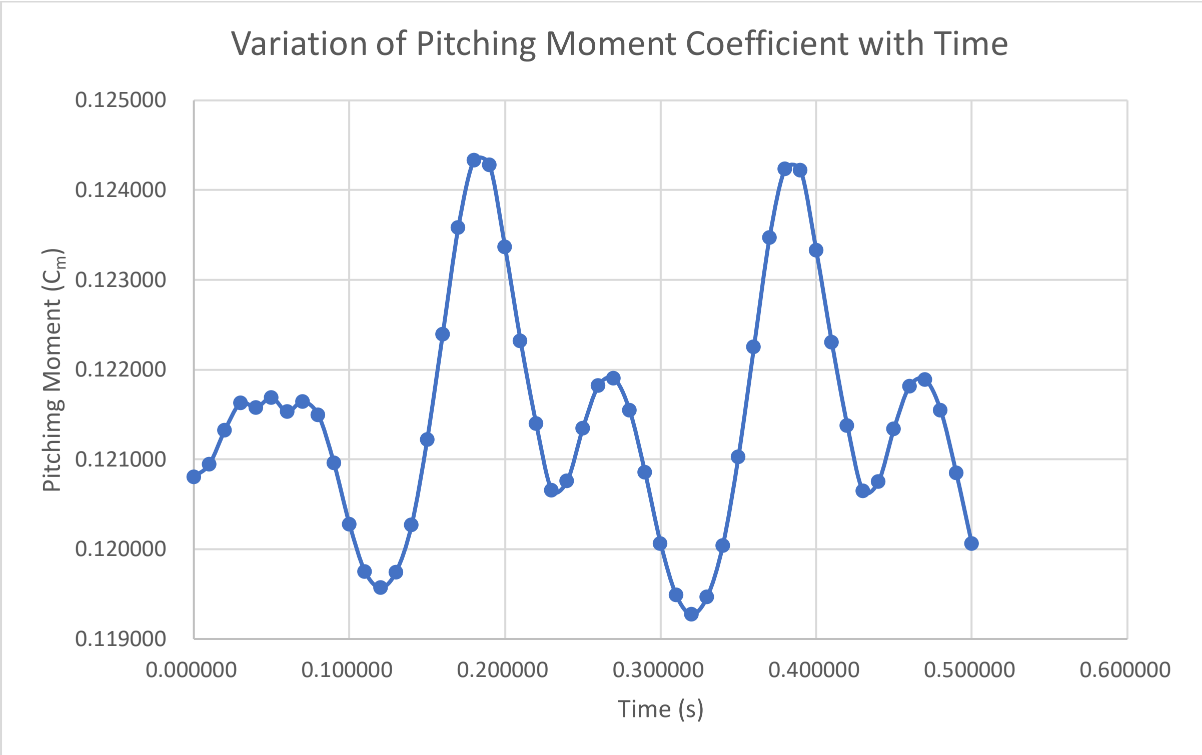

Figure 4.7(a): Plotted graph shows how the pitching moment coefficient (C_m) varied with time over the course of the simulation.

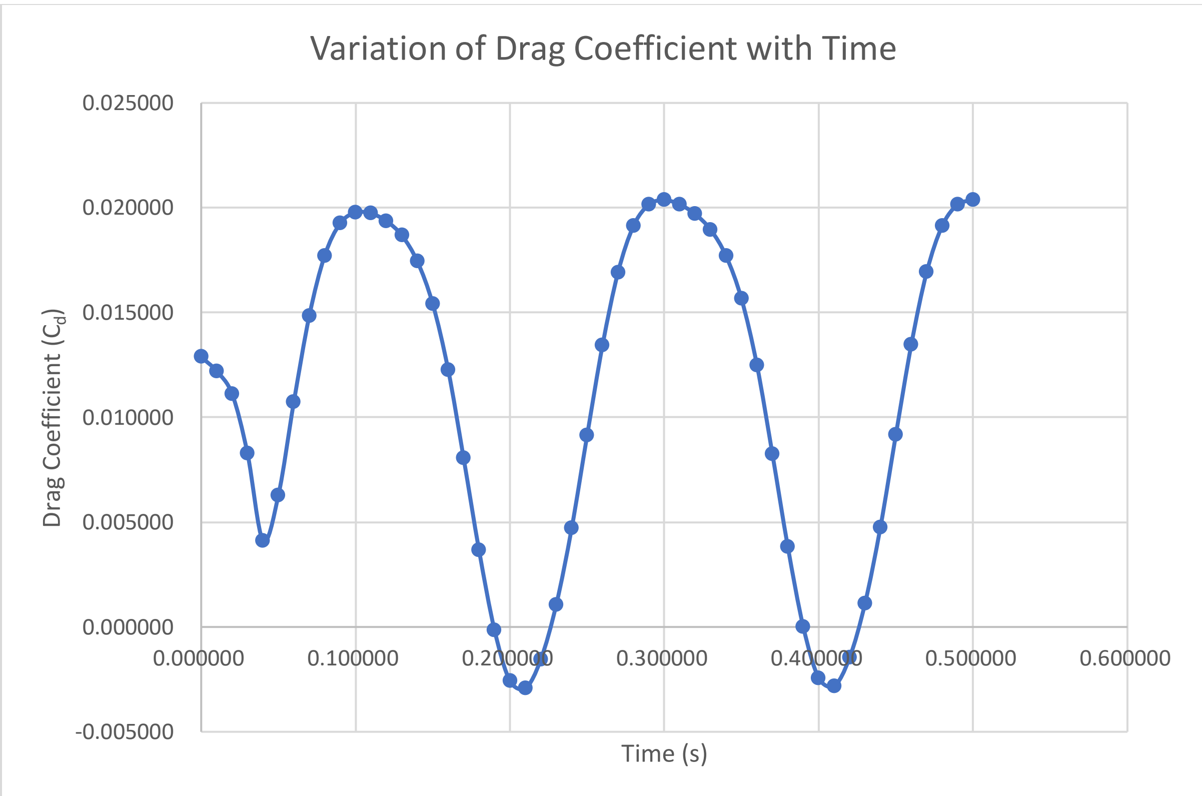

Figure 4.7(b): Plotted graph shows how the drag coefficient (C_d) varied with time over the course of the simulation.

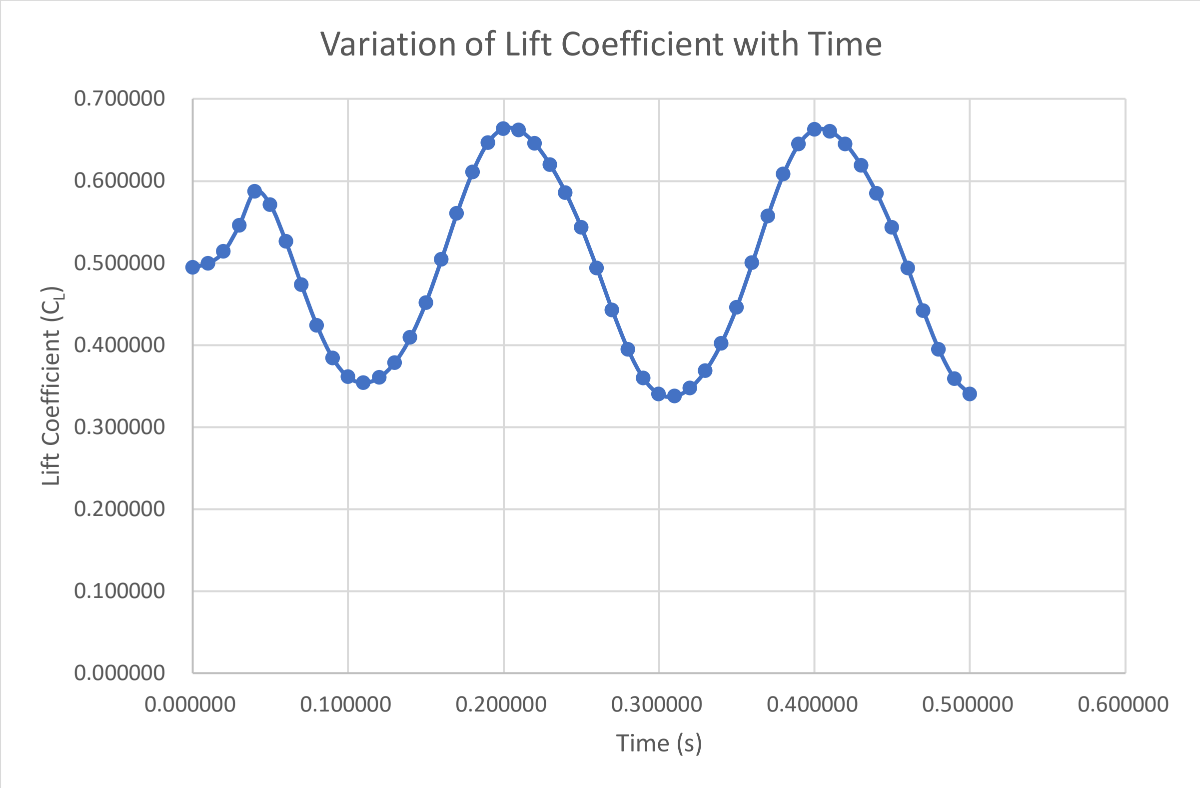

Figure 4.7(c): Plotted graph shows how the lift coefficient (C_L) varied with time over the course of the simulation.

Case 2.

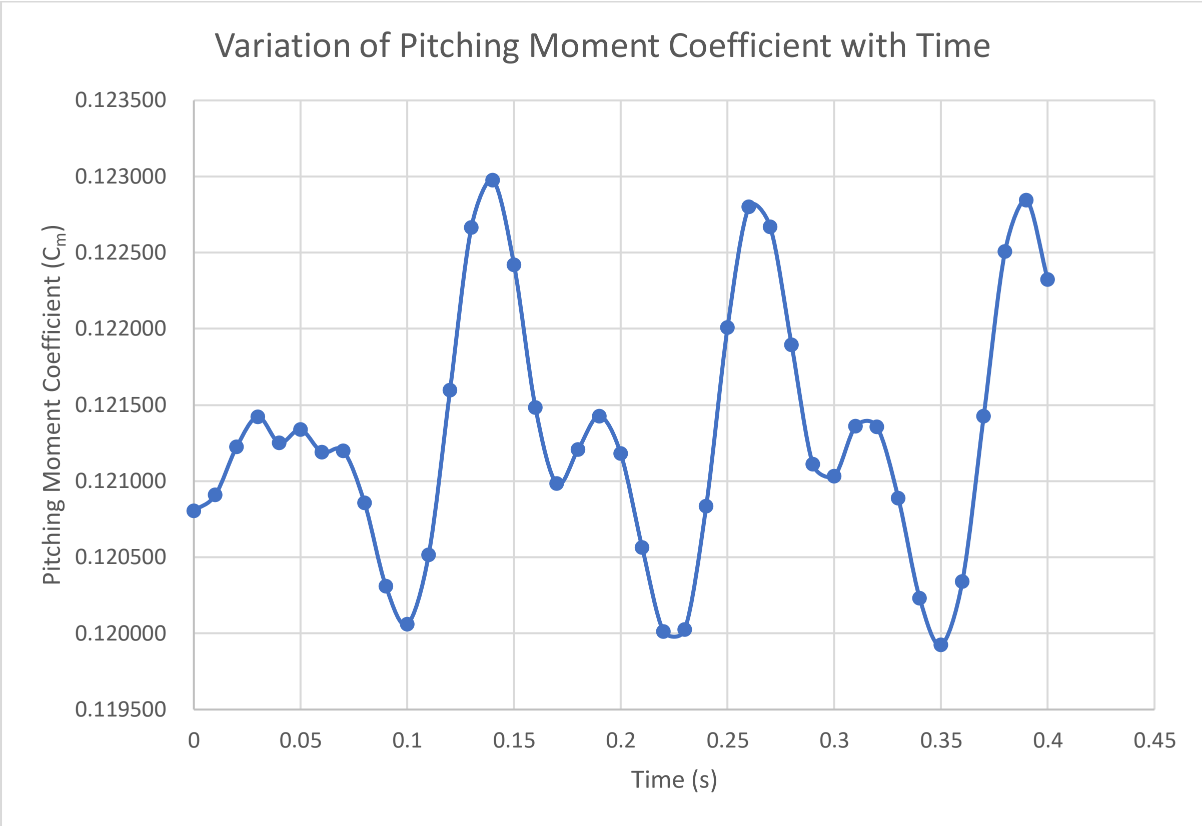

Figure 4.8(a): Plotted graph shows how the pitching moment coefficient (C_m) varied with time over the course of the Atassi gust for a frequency of f = 8Hz & freestream velocity of U_∞ = 25m/s.

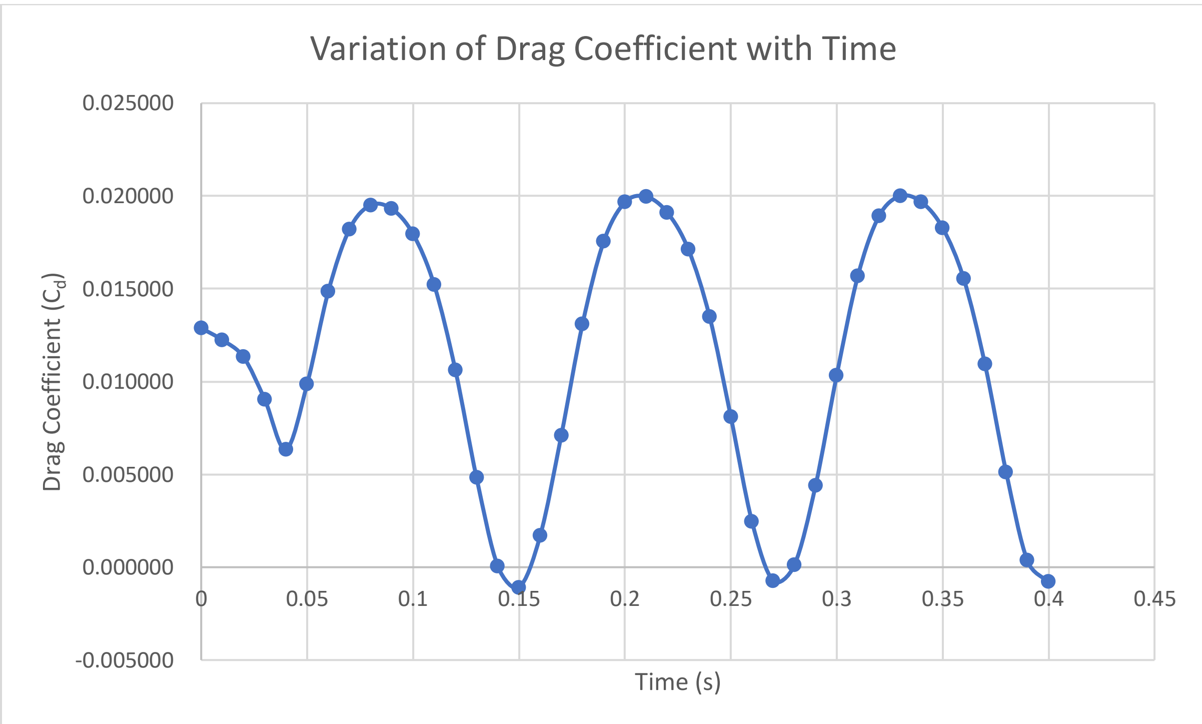

Figure 4.8(b): Plotted graph shows how the drag coefficient (C_d) varied with time over the course of the simulation for a frequency of f = 8Hz & freestream velocity of U_∞ = 25m/s.

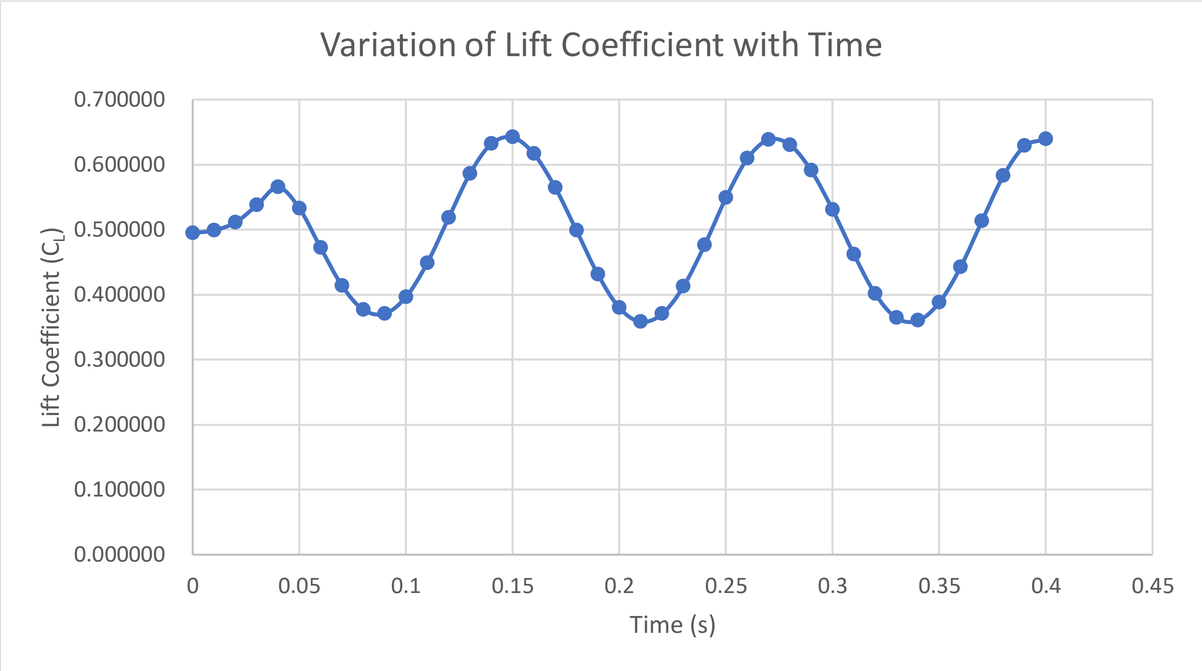

Figure 4.8(c): Plotted graph shows how the lift coefficient (C_L) varied with time over the course of the simulation for a frequency of f = 8Hz & freestream velocity of U_∞ = 25m/s.

Case 3.

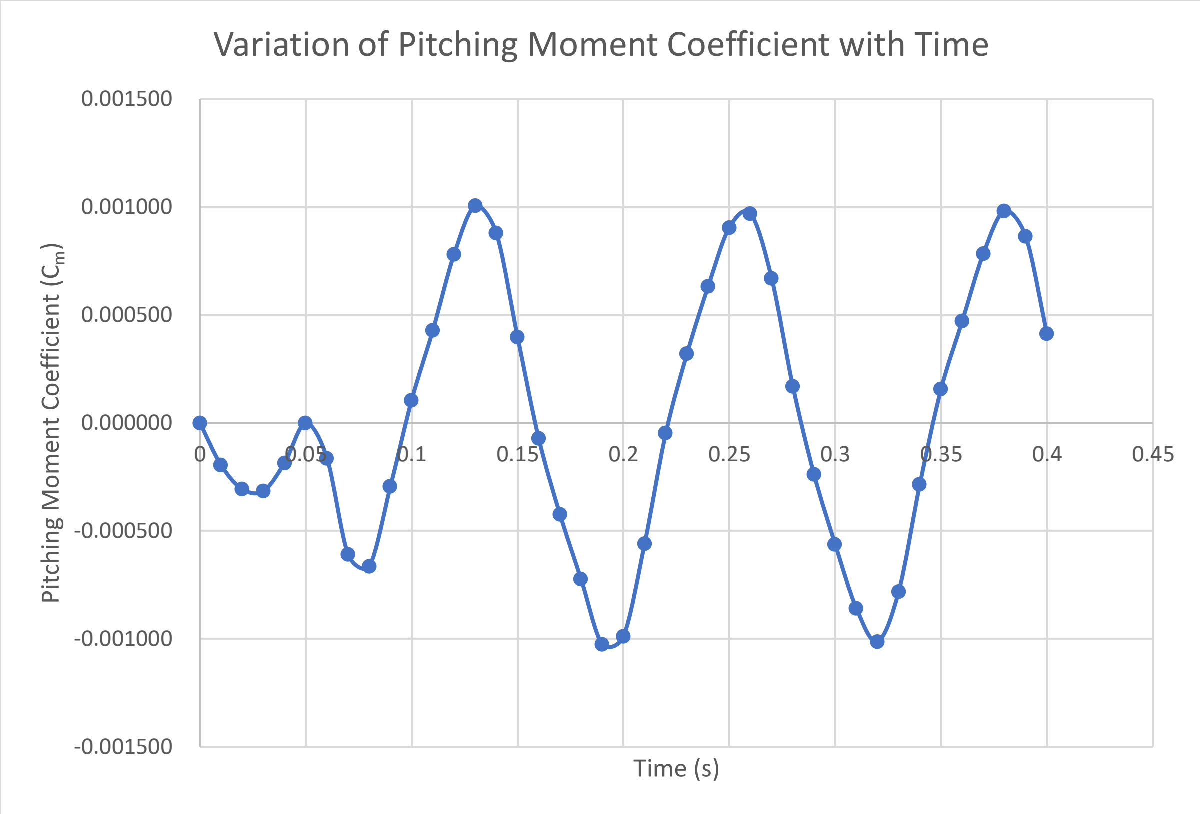

Figure 4.9(a): Plotted graph shows how the pitching moment coefficient (C_m) varied with time over the course of the Sears gust for a frequency of f = 8Hz & freestream velocity of U_∞ = 20m/s.

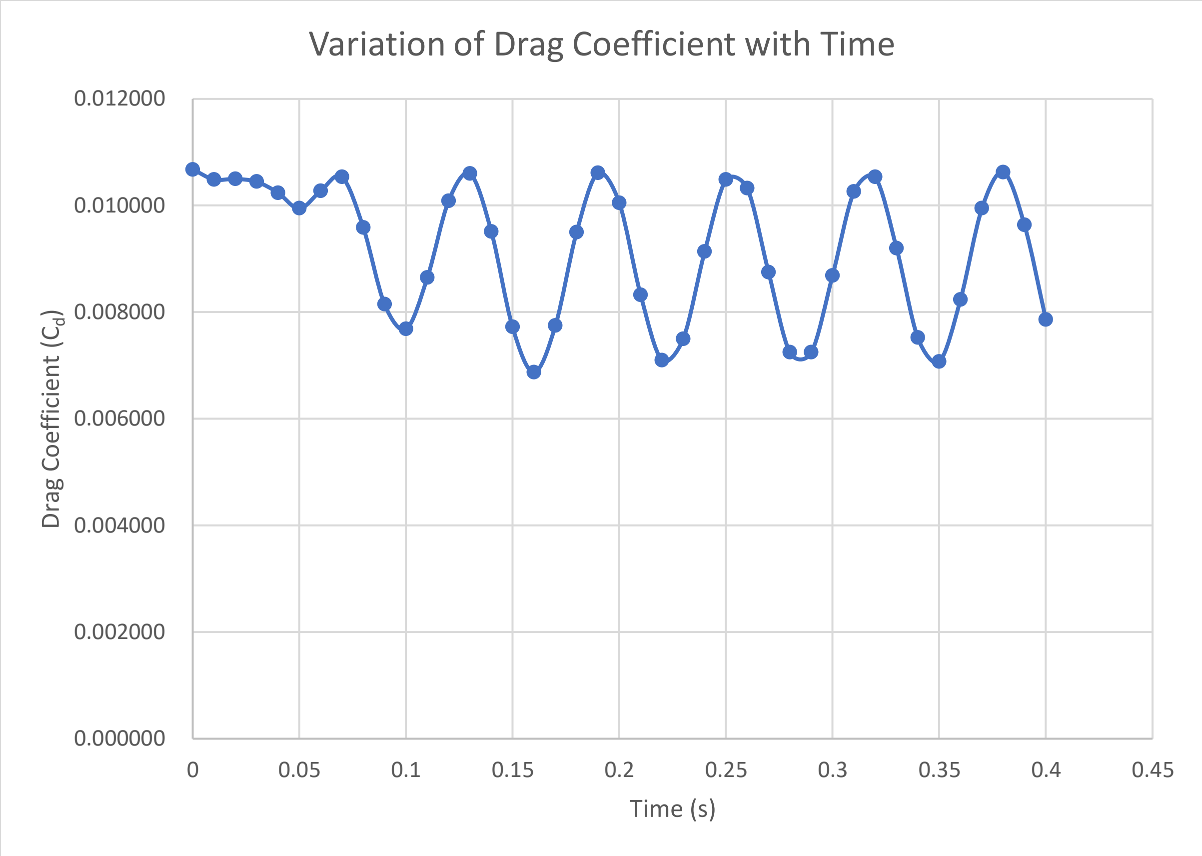

Figure 4.9(b): Plotted graph shows how the drag coefficient (C_d) varied with time over the course of the simulation for a frequency of f = 8Hz & freestream velocity of U_∞ = 20m/s.

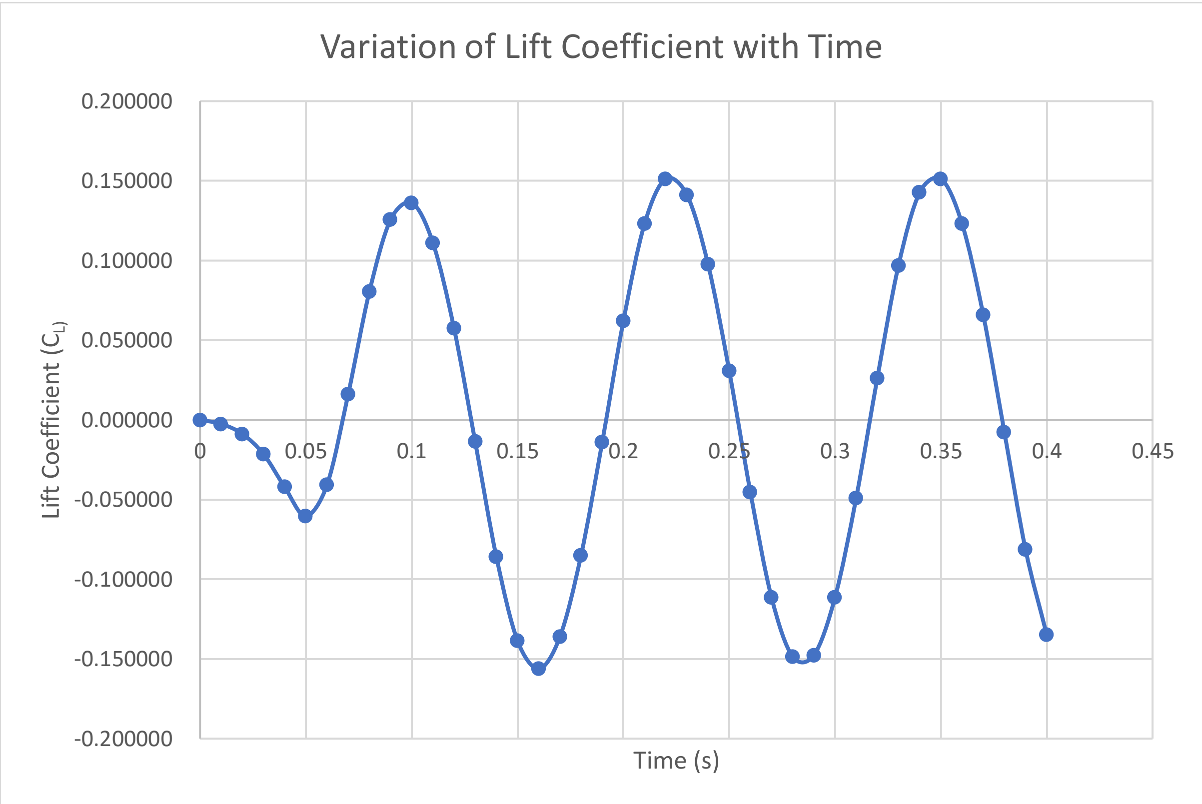

Figure 4.9(c): Plotted graph shows how the lift coefficient (C_L) varied with time over the course of the simulation for a frequency of f = 8Hz & freestream velocity of U_∞ = 20m/s.

As implied by the topic of research for this paper, the work done was to analyse the aerodynamics of an aircraft in gusty inflow conditions. An aircraft's motion in flight is heavily dependent on the engines and wings. The latter plays an immense role in the way the aircraft interacts with moving air while being in motion, simultaneously. As mentioned before, this is the basis of aerodynamics. The flow field of air around an airfoil, at different speeds and frequencies was studied. The following subsection shows the comparisons made of results obtained for each respective case in this paper with those from previous researchers.

4.3 Review of Graphed Results

The previous section shows the simulation results obtained for the respective cases. The Atassi and Sears inflow fields were characterized by oscillating vanes. For the first case, at a frequency of f = 5Hz, gust angle of 2° and a freestream velocity of 25m/s, the flow field of the velocity (U) in Fig. 4.1(a) to (h) shows a consistency with the results obtained from the data provided by Wu *et al* (2020). The graphs given in Fig. 4.7(a), (b) & (c) show the trends of how the pitching moment coefficient (C_m), drag coefficient (C_d) and lift coefficient (C_L) vary with time, respectively. Comparing this data with that from Wu *et al* (2020), similarities can be found. The curves in Fig. 1.5 in the first chapter do not show much deviation with those in Fig. 4.7(a), (b) & (c). The same is true for those in Fig. 4.8(a), (b) & (c). These curves result from a simulation with similar parameters except for the frequency, which is f = 8Hz. The work done by Wu *et al* (2020) gives results for simulations executed at various gust angle values, in the range of $0° \leq \alpha \leq 8°$, as opposed to the one carried out in this paper, where the gust angle implemented for all cases is α = 2°.

The second case was simulated and naturally, the results did not show a large disparity with those obtained in the latter. The discrepancy arose from the fact that the frequency input was the only differing factor. The same gust angle and freestream velocity, and a frequency of f = 8Hz produced the velocity flow fields shown in Figs. 4.3(a) to (f) after a period (T) of 0.125s for each oscillation. The results achieved in this research are not novel. As mentioned before, an experiment was conducted by Wei *et al* (2019) in an attempt to investigate the same aspects as those in this paper and, as implied previously, simulations similar to the ones carried out in this research were performed by Wu *et al* (2020). Like Wei *et al* (2019) and Wu *et al* (2020), the results achieved in this paper show that the normalized lift responses to the Atassi inflows conform to the Sears function [2], [8]. The differing factor in the running of Case 1 & 2 was the gust frequency (f). It can be seen by comparison that, the slightly higher frequency applied in the second case resulted in a slightly larger amplitude of the pitching moment coefficient (Fig. 4.7(a) and Fig. 4.8(a)). For the third case in which Sears inflow conditions are applied, the initial trend of the coefficient curves (C_m, C_d & C_L) is different from the ones formed in the other two cases. Moreover, it is seen that the drag coefficient between the two Atassi gusty inflow cases differs in amplitude. By observing figure 4.7(b) and 4.8(b), the previous statement can deduced. What supports this hypothesis is the fact that, at a lower frequency in case 1 (5Hz) than case 2 (8Hz), there is a bigger separation of the flow at the test airfoil's trailing edge. This results in an increase in drag and consequently, an increase in the drag coefficient. The reverse is true for case 2 in which the frequency (8Hz) is higher, meaning that there is a reduction in flow separation at the same spot of the test airfoil in this scenario. This yields less drag and inturn, a reduction of the drag coefficient as seen by the smaller amplitude in Fig. 4.8(b) than the one in Fig. 4.7(b).

An observation made in the research results of this paper, shown in Fig. 4.7(c), Fig. 4.8(c) and Fig. 4.9(c) is the linearity of the lift coefficient (C_L) curves. The trend of the figures is linear and does not show any distortion. The reason for this is the reduced level of vigour of the wake induced flow separation. It can therefore be concluded that the airfoil inflow is sinusoidal and consequently, by analysing the streamlines in Fig. 4.6, it is evidently clear that the flow is devoid of any separation. The Sears gust inflow frequency value of f = 8Hz is higher than the ones incorporated by Wu *et al* (2020) for the Sears inflow case. Results in the experiments carried out by Wu *et al* (2020) and Wei *et al* (2019), along with those obtained in this paper, are consistent with the theoretical statement that implies the decrease of turbulent wakes and flow separation with an increase in gust inflow frequency.

Chapter 5: Conclusion & Recommendations for Future Work

5.1 Conclusion

The process of investigating aircraft aerodynamics in gusty inflow conditions makes one susceptible to learning the operation of certain engineering software, particularly within the computational fluid dynamics (CFD) domain. This research was conducted to observe and analyse how an aircraft, particularly the airfoils, react to turbulent airflow and to give a surface level idea on how aircraft structures are affected throughout this process. The basis of flight is to manouvre off the ground, in air and this is made possible when sufficient lift force is generated around an airfoil. The magnitude of this force is affected by conditions such as turbulence but rarely at a level high enough to adversely affect it i.e as seen from the results obtained in this thesis, there will always be a constant fluctuation of the forces (lift & drag) and inherently, the corresponding aerodynamic coefficients. It is important to note that, the Atassi function mentioned in this paper can be used to formulate a gust that flows horizontally. The gust response of the test airfoil is greatly affected by this turbulent flow (gust) and this only happens at reduced frequencies which are low. In gust response analysis, the airfoil thickness is not factored into the calculations and observations and this is therefore an inhibition of the Atassi function. Simulations were run using OpenFOAM 8 software which is a part of the computational fluid dynamics package. The partitioning of the respective simulation cases inorder to run them through parallel processing enabled the overall simulation window to be shortened. Increasing the size of the time-step (`deltaT`) made this feasible. It was imperative for the mesh to be decomposed into different sections i.e., 4 processors. Although this critical step was implemented, the simulations were still lengthy.

5.2 Recommendations for Future Work

Gust is a phenomenon that affects all non-human moving objects, from cars, birds, motorbikes to aircraft and space shuttles. The author of this work was inevitably exposed to the myriad of research work that has been done in this field previously. An observation made was the lack of research work that investigates and provides conclusive results on gust response of Formula 1 cars and the inter-sharing of knowledge between engineers or aerodynamicists in the latter industry and, in aerospace. Exploration of this avenue was done because of how the two types of vehicles, F1 cars and aircraft, require the same type of force but applied inversely to execute their primary purpose. It is imperative for there to be future simulations, computations and/or calculations for cases that incorporate larger gust inflow angles. Based on the concluding remarks of this paper, the formulation of a solver that processes at a faster rate than the pimpleFoam solver should perhaps be done in due course. Furthermore, the author believes that more work should be done to enhance the use of software within the computational fluid dynamics (CFD) package for simulations for wind tunnels, numerically.

References

[1] Z. Wu, Y. Cao, M. Ismail, "*Gust Loads On Aircraft*", The Aeronautical Journal No. 1266, Volume 123, August 2019.

[2] N. J Wei, J. Kissing, T.T.B Wester, S. Wegt, K. Schiffman, S. Jakirlic, M. Holling, J. Peinke, C. Tropea, "*Insights into the Periodic Gust Response of Airfoils*", J. Fluid Mech. Vol. 876, pp. 237-263, 2019.

[3] P. D. Lysak, D. E. Capone, M. L. Jonson, "*Prediction of High Frequency Gust Response with Airfoil Thickness Effects*", J. Fluids Struct. 39, pp. 258, 2013.

[4] P. Lamson, "*Measurement of Lift Fluctuations Due to Turbulence*", Technical Note 3880, National Advisory Committee for Aeronautics, March 1957.

[5] S. Li, M. Li, H. Liao, "*The Lift on an Aerofoil in Grid-Generated Turbulence*", J. Fluid Mech. 771, pp. 16, 2015.

[6] J. P. Giesing, W. P. Rodden, B. Stahl, "Sears Function & Lifting Surface Theory for Harmonic Gust Fields", J. Aircraft Vol. 7, No. 3, pp. 252-255, May 1970.

[7] D. Traphan, T. T. B. Wester, J. Peinke, G. Gulker, "*On the Aerodynamic Behaviour of an Airfoil Under Tailored Turbulent Inflow Conditions*", Conference Paper, 5th International Conference on Experimental Fluid Mechanics (ICEFM), Munich, Germany, July 2018.

[8] W. Zhenlong, G. Bangga, T. Lutz, G. Kampers, M. Holling, "*Insights Into Airfoil Response to Sinusoidal Gusty Inflow by Oscillating Vanes*", Phys. Fluids 32, pp. 125107, 2020.

[9] U. Cordes, G. Kampers, T. Meibner, C. Tropea, J. Peinke, M. Holling, "*Note on the Limitations of the Theodorsen & Sears Functions*", J. Fluid Mech. Vol. 811, pp. R1-R11, 2017.

[10] M. Massaro & J. M. R. Graham, "*The Effect of Three-Dimensionality on the Aerodynamic Admittance of Thin Sections in Freestream Turbulence*", J. Fluids Struct. 57, pp. 81-90, 2015.

[11] R. W. Paterson, R. K. Amiet, "*Noise and Surface Pressure Response of an Airfoil to Incident Turbulence*", J. Aircr. 14, pp. 729-736, 1977.

[12] R. K. Amiet, "*Acoustic Radiation From an Airfoil in a Turbulent Stream*", J. Sound Vib. 41, pp. 407-420,1975.

[13] J. O. Hinze, "*Turbulence*", McGraw-Hill 2nd Ed., New York, 1975.

[14] W. R. Sears, “*Some Aspects of Non-Stationery Airfoil Theory and its Practical Application*”, J. Aeronaut. Sci. 8, pp. 104-108, 1941.

[15] P. M.G. J. Lancelot, J. Sodja, N. P. M. Werter, R. De Breuker, “Design and Testing of a Low Subsonic Wind Tunnel Gust Generator”, Advances in Aircraft and Spacecraft Science, Vol. 4, No. 2, pp. 125-144, 2017.

[16] G. L. Commerford, F. O. Carta, “*Unsteady Aerodynamic Response of a Two-Dimensional Airfoil at High Reduced Frequency*”, AIAA Journal Vol. 12 No. 1, January 1974.

[17] G. L. Larose, “*Experimental Determination of the Aerodynamic Admittance of a Bridge Deck Segment*”, Journal of Fluids & Structures 13, pp. 1029-1040, 1999.

[18] R. Aris, “*Vectors, Tensors and the Basic Equations*”, Journal of Fluid Mechanics, Dover Publications, 1989.

[19] Wolf Dynamics, “*Finite Volume Method: A Crash Introduction*”. Accessed 05.08.21. http://www.wolfdynamics.com/wiki/fvm_crash_intro.pdf

Appendix A OpenFOAM Input Files

A1

As observed in the paper, the software used for simulations in this overall investigation was OpenFOAM 8. A table is given further ahead to show the initial value used to define the 1st case which is 'Wing Motion 2D_pimpleFoam_Gust Angle2' for velocity (U) = 25m/s & frequency (f) = 5Hz. The respective contents of the files shown in this table are provided.

<u>Case 1</u>

A1.1: Contents of the file \0\k

```
/*--------------------------------*- C++ -*----------------------------------*\
  =========                 |
  \\      /  F ield         | OpenFOAM: The Open Source CFD Toolbox
   \\    /   O peration     | Website:  https://openfoam.org
    \\  /    A nd           | Version:  6
     \\/     M anipulation  |
\*---------------------------------------------------------------------------*/
FoamFile
{
    version     2.0;
    format      ascii;
    class       volScalarField;
    location    "0";
    object      k;
}
// * * * * * * * * * * * * * * * * * * * * * * * * * * * * * * * * * * * * * //

dimensions      [0 2 -2 0 0 0 0];

internalField   nonuniform List<scalar>
278155
(
9.77652e-07
9.78316e-07
```

```
9.76997e-07
9.78975e-07
9.7767e-07
9.75792e-07
9.79628e-07
9.78338e-07
9.76476e-07
9.74676e-07
9.80277e-07
9.79e-07
9.77155e-07
9.75374e-07
9.73227e-07
9.8092e-07
```

**Due to the file being large, contents/values up to line 16 are shown.*

A1.2: Contents of the file \0\nut

```
/*--------------------------------*- C++ -*----------------------------------*\
  =========                 |
  \\      /  F ield         | OpenFOAM: The Open Source CFD Toolbox
   \\    /   O peration     | Website:  https://openfoam.org
    \\  /    A nd           | Version:  6
     \\/     M anipulation  |
\*---------------------------------------------------------------------------*/
FoamFile
{
    version     2.0;
    format      ascii;
    class       volScalarField;
    location    "0";
    object      nut;
}
// * * * * * * * * * * * * * * * * * * * * * * * * * * * * * * * * * * * * * //

dimensions      [0 2 -1 0 0 0 0];
```

```
internalField   nonuniform List<scalar>
278155
(
5.14924e-07
5.14985e-07
5.07495e-07
5.15045e-07
5.07555e-07
4.97459e-07
5.15105e-07
5.07613e-07
4.97518e-07
4.86645e-07
5.15165e-07
5.07672e-07
4.97576e-07
4.86704e-07
4.75741e-07
5.15224e-07
```

**Due to the file being large, contents/values up to line 16 are shown.*

A1.3: Contents of the file \0\omega

```
/*--------------------------------*- C++ -*----------------------------------
--*\
  =========                 |
  \\      /  F ield         | OpenFOAM: The Open Source CFD Toolbox
   \\    /   O peration     | Website:  https://openfoam.org
    \\  /    A nd           | Version:  6
     \\/     M anipulation  |
\*---------------------------------------------------------------------------
--*/
FoamFile
{
    version     2.0;
    format      ascii;
```

```
    class       volScalarField;
    location    "0";
    object      omega;
}
// * * * * * * * * * * * * * * * * * * * * * * * * * * * * * * * * * * * * *
* //

dimensions      [0 0 -1 0 0 0 0];

internalField   nonuniform List<scalar>
278155
(
1.89863
1.8997
1.92514
1.90076
1.92624
1.96155
1.9018
1.92733
1.9627
2.00285
1.90284
1.92841
1.96383
2.00404
2.04571
1.90387
```

**Due to the file being large, contents/values up to line 16 are shown.*

A1.4: Contents of the file \0\p

```
/*--------------------------------*- C++ -*----------------------------------
--*\
  =========                 |
  \\      /  F ield         | OpenFOAM: The Open Source CFD Toolbox
   \\    /   O peration     | Website:  https://openfoam.org
    \\  /    A nd           | Version:  6
     \\/     M anipulation  |
```

```
\*---------------------------------------------------------------------------
--*/
FoamFile
{
    version     2.0;
    format      ascii;
    class       volScalarField;
    location    "0";
    object      p;
}
// * * * * * * * * * * * * * * * * * * * * * * * * * * * * * * * * * * * * *
* //

dimensions      [0 2 -2 0 0 0 0];

internalField   nonuniform List<scalar>
278155
(
-0.000222363
-0.000456109
-0.000207439
-0.000794842
-0.0004402
-0.000232654
-0.00108318
-0.000778922
-0.000464779
-0.000206383
-0.00137326
-0.00106697
-0.000804198
-0.000436607
-0.000235494
-0.00165035
```

**Due to the file being large, contents/values up to line 16 are shown.*

A1.5: Contents of the file \0\pointDisplacement

```
/*--------------------------------*- C++ -*----------------------------------*\
  =========                 |
  \\      /  F ield         | OpenFOAM: The Open Source CFD Toolbox
   \\    /   O peration     | Website:  https://openfoam.org
    \\  /    A nd           | Version:  6
     \\/     M anipulation  |
\*---------------------------------------------------------------------------*/
FoamFile
{
    version     2.0;
    format      ascii;
    class       pointVectorField;
    location    "0.01";
    object      pointDisplacement;
}
// * * * * * * * * * * * * * * * * * * * * * * * * * * * * * * * * * * * * * //

dimensions      [0 1 0 0 0 0 0];

internalField   uniform (0 0 0);

boundaryField
{
    vane1
    {
        type            angularOscillatingDisplacement;
        value           uniform (0 0 0);
        axis            (0 0 1);
        origin          (-1.1 0.33 0);
        angle0          0;
        amplitude       0.1391;
        omega           -31.42;
    }

    vane2
```

```
{
    type            angularOscillatingDisplacement;
    value           uniform (0 0 0);
    axis            (0 0 1);
    origin          (-1.1 0.11 0);
    angle0          0;
    amplitude       0.1391;
    omega           -31.42;
}

vane3
{
    type            angularOscillatingDisplacement;
    value           uniform (0 0 0);
    axis            (0 0 1);
    origin          (-1.1 -0.11 0);
    angle0          0;
    amplitude       0.1391;
    omega           -31.42;
}

vane4
{
    type            angularOscillatingDisplacement;
    value           uniform (0 0 0);
    axis            (0 0 1);
    origin          (-1.1 -0.33 0);
    angle0          0;
    amplitude       0.1391;
    omega           -31.42;
}

front
{
    type            empty;
}

back
{
    type            empty;
```

```
    }

    ".*"
    {
        type            fixedValue;
        value           uniform (0 0 0);
    }
}


//
*************************************************************************
//
```

A1.6: Contents of the file \0\U

```
/*--------------------------------*- C++ -*----------------------------------
--*\
  =========                 |
  \\      /  F ield         | OpenFOAM: The Open Source CFD Toolbox
   \\    /   O peration     | Website:  https://openfoam.org
    \\  /    A nd           | Version:  6
     \\/     M anipulation  |
\*---------------------------------------------------------------------------
--*/
FoamFile
{
    version     2.0;
    format      ascii;
    class       volVectorField;
    location    "0";
    object      U;
}
// * * * * * * * * * * * * * * * * * * * * * * * * * * * * * * * * * * * * *
* //

dimensions      [0 1 -1 0 0 0 0];

internalField   nonuniform List<vector>
278155
```

```
(
(25.1726 0.000602053 0)
(25.1726 0.000610236 0)
(25.1725 -0.000508467 0)
(25.1726 0.000614727 0)
(25.1725 -0.000516097 0)
(25.1726 0.000431344 0)
(25.1726 0.000620048 0)
(25.1725 -0.000519782 0)
(25.1726 0.000436718 0)
(25.1725 -0.000349768 0)
(25.1726 0.0006252 0)
(25.1725 -0.00052452 0)
(25.1726 0.000440162 0)
(25.1725 -0.000355955 0)
(25.1726 0.0002952 0)
(25.1726 0.000630417 0)
```

Due to the file being large, contents/values up to line 16 are shown.

A2: Input Value Table

Table A2.1: List of relevant files and structure of the folders for the OpenFOAM (Atassi Gust), Case 1.

Directory Name	File Name	Sub-Directory	File Contents
\0			
	k		Turbulent Kinetic Energy.
	nut		Turbulence Viscosity.
	omega		Turbulent Dissipation Rate.
	p		Pressure.
	pointDisplacement		Values for Point Vector Field.
	U		Velocity.
\constant			
	dynamicMeshDict		Controls the deformation & morphing of the mesh during a simulation.
	transportProperties		Definition of transport properties.

Directory Name	File Name	Sub-Directory	File Contents
	turbulenceProperties		Selection of LES/Laminar/URANS simulation.
		\PolyMesh	Definition of the mesh to be used.
\system			
	controlDict		Parameters for controlling time and the reading & writing of data.
	decomposeParDict		Parameters for controlling the mesh decomposition.
	fvSchemes		Definition of the discretization schemes.
	fvSolution		Residual tolerances & the equation solvers defined.
	topoSetDict		Parameters for post processing and sampling locations.

Appendix B Aerodynamic Coefficient Values per case

Table B1.1: Case 1 values for the respective aerodynamic coefficients calculated during the simulation.

Time(s)	C_m	C_d	C_L
0	0,120806	0,012882	0,494688
0,01	0,120948	0,012204	0,499397
0,02	0,121329	0,011121	0,513558
0,03	0,121628	0,008277	0,545923
0,04	0,121577	0,004126	0,586995
0,05	0,121688	0,006278	0,570691
0,06	0,121530	0,010730	0,525789
0,07	0,121646	0,014837	0,473272
0,08	0,121495	0,017715	0,423383
0,09	0,120963	0,019252	0,384140
0,1	0,120281	0,019772	0,360788
0,11	0,119752	0,019727	0,353738
0,12	0,119570	0,019363	0,360258
0,13	0,119747	0,018676	0,378433
0,14	0,120272	0,017440	0,408763
0,15	0,121225	0,015410	0,451257
0,16	0,122398	0,012263	0,503777
0,17	0,123585	0,008055	0,560034
0,18	0,124330	0,003652	0,610292
0,19	0,124284	-0,000148	0,646695
0,2	0,123365	-0,002573	0,663668
0,21	0,122322	-0,002929	0,661437
0,22	0,121401	-0,001549	0,645656
0,23	0,120660	0,001063	0,619472
0,24	0,120761	0,004714	0,585191
0,25	0,121345	0,009136	0,543135
0,26	0,121820	0,013449	0,493901
0,27	0,121902	0,016910	0,441956
0,28	0,121552	0,019127	0,394618
0,29	0,120856	0,020145	0,359177
0,3	0,120065	0,020366	0,340011
0,31	0,119490	0,020155	0,337151
0,32	0,119273	0,019692	0,347418
0,33	0,119470	0,018951	0,368751
0,34	0,120044	0,017698	0,401542
0,35	0,121030	0,015650	0,445855

Time(s)	C_m	C_d	C_L
0,36	0,122252	0,012493	0,499755
0,37	0,123470	0,008258	0,556999
0,38	0,124237	0,003825	0,607990
0,39	0,124220	0,000012	0,644926
0,4	0,123330	-0,002432	0,662278
0,41	0,122308	-0,002822	0,660409
0,42	0,121377	-0,001472	0,644872
0,43	0,120651	0,001121	0,618885
0,44	0,120751	0,004761	0,584750
0,45	0,121343	0,009170	0,542751
0,46	0,121817	0,013473	0,493542
0,47	0,121891	0,016933	0,441693
0,48	0,121546	0,019133	0,394397
0,49	0,120850	0,020148	0,358990
0,5	0,120061	0,020367	0,339913

Table B1.2: Case 2 values for the respective aerodynamic coefficients calculated during the simulation.

Time(s)	C_m	C_d	C_L
0	0,120806	0,012882	0,494688
0,01	0,120908	0,012239	0,498812
0,02	0,121223	0,011318	0,510887
0,03	0,121422	0,009036	0,537097
0,04	0,121252	0,006346	0,565112
0,05	0,121338	0,009864	0,532775
0,06	0,121189	0,014855	0,472053
0,07	0,121198	0,018209	0,413717
0,08	0,120855	0,019505	0,376769
0,09	0,120308	0,019300	0,370779
0,1	0,120060	0,017954	0,396409
0,11	0,120515	0,015205	0,448756
0,12	0,121595	0,010620	0,517934
0,13	0,122666	0,004811	0,586119
0,14	0,122977	0,000060	0,631690
0,15	0,122420	-0,001091	0,641708
0,16	0,121484	0,001687	0,616197
0,17	0,120984	0,007109	0,564370
0,18	0,121207	0,013097	0,498172
0,19	0,121427	0,017543	0,430846
0,2	0,121179	0,019655	0,379740
0,21	0,120565	0,019964	0,358281

Time(s)	C_m	C_d	C_L
0,22	0,120014	0,019113	0,370168
0,23	0,120025	0,017115	0,411991
0,24	0,120835	0,013492	0,475989
0,25	0,122009	0,008108	0,548705
0,26	0,122800	0,002456	0,608955
0,27	0,122670	-0,000732	0,638156
0,28	0,121896	0,000112	0,630295
0,29	0,121110	0,004388	0,590630
0,3	0,121033	0,010339	0,530499
0,31	0,121359	0,015698	0,462055
0,32	0,121356	0,018923	0,401085
0,33	0,120889	0,019998	0,364103
0,34	0,120232	0,019670	0,359840
0,35	0,119922	0,018280	0,387723
0,36	0,120341	0,015523	0,442200
0,37	0,121426	0,010928	0,512955
0,38	0,122509	0,005114	0,582158
0,39	0,122844	0,000358	0,628293
0,4	0,122322	-0,000792	0,638602

Table B1.3: Case 3 values for the respective aerodynamic coefficients calculated during the simulation.

Time(s)	C_m	C_d	C_L
0	0,000000	0,010678	0,000002
0,01	-0,000196	0,010489	-0,002525
0,02	-0,000306	0,010500	-0,008822
0,03	-0,000315	0,010445	-0,021458
0,04	-0,000184	0,010240	-0,042189
0,05	0,000000	0,009943	-0,060405
0,06	-0,000162	0,010274	-0,040807
0,07	-0,000609	0,010535	0,016127
0,08	-0,000663	0,009586	0,080361
0,09	-0,000293	0,008143	0,125542
0,1	0,000106	0,007680	0,136241
0,11	0,000429	0,008645	0,111195
0,12	0,000780	0,010087	0,057479
0,13	0,001005	0,010598	-0,013717
0,14	0,000879	0,009515	-0,085885
0,15	0,000399	0,007716	-0,138609
0,16	-0,000072	0,006875	-0,156237

Time(s)	C_m	C_d	C_L
0,17	-0,000422	0,007741	-0,136197
0,18	-0,000723	0,009501	-0,085038
0,19	-0,001026	0,010610	-0,014072
0,2	-0,000989	0,010052	0,061926
0,21	-0,000560	0,008325	0,122978
0,22	-0,000048	0,007101	0,151318
0,23	0,000320	0,007503	0,141289
0,24	0,000632	0,009130	0,097663
0,25	0,000905	0,010480	0,030795
0,26	0,000970	0,010323	-0,045272
0,27	0,000671	0,008746	-0,111414
0,28	0,000171	0,007244	-0,148569
0,29	-0,000237	0,007243	-0,147646
0,3	-0,000561	0,008688	-0,111337
0,31	-0,000858	0,010255	-0,048988
0,32	-0,001012	0,010530	0,026359
0,33	-0,000781	0,009202	0,096998
0,34	-0,000283	0,007517	0,142744
0,35	0,000157	0,007070	0,151354
0,36	0,000472	0,008240	0,123128
0,37	0,000785	0,009944	0,066068
0,38	0,000984	0,010625	-0,007596
0,39	0,000864	0,009631	-0,081280
0,4	0,000414	0,007863	-0,134675

ACKNOWLEDGEMENTS

I would first like to thank my supervisor/advisor, Zhenlong Wu, for his endless help and the invaluable guidance he offered me to ensure that I execute the work to the best of my ability.

I would also like to thank the lecturers and professors who have taught me in various subjects/courses at Nanjing University of Aeronautics & Astronautics over the past 4 years, many of which have helped to shape my engineering skills.

I extend my thanks to the OpenFOAM community on the various internet platforms worldwide, whose tips and advice enabled me to use the software with considerable ease.

My sincere gratitude is extended to the multiple researchers who have carried out work in the past, in a similar capacity to that which I have done. Their work laid a solid foundation for me to build from.

I thank my dear mother for providing me with unparalleled support and priceless knowledge during this whole process.

Lastly, I thank God Almighty for gracing me with the tangible and intangible tools needed for me to cross over this final hurdle and put my best foot forward.

This thesis is dedicated to two dear uncles of mine who have inspired me to pursue a career in the field of engineering, one of whom is passionate about the field of aerodynamics as much as I am.